Picosecond photofragment spectroscopy. I. Microcanonical state-to-state rates of the reaction NCNO→CN+NO

Lutfur R. Khundkar, Joseph L. Knee, and Ahmed H. Zewail

Citation: The Journal of Chemical Physics **87**, 77 (1987); doi: 10.1063/1.453527
View online: http://dx.doi.org/10.1063/1.453527
View Table of Contents: http://scitation.aip.org/content/aip/journal/jcp/87/1?ver=pdfcov
Published by the AIP Publishing

Picosecond photofragment spectroscopy. I. Microcanonical state-to-state rates of the reaction NCNO→CN+NO

Lutfur R. Khundkar, Joseph L. Knee,[a] and Ahmed H. Zewail
Arthur Amos Noyes Laboratory of Chemical Physics,[b] California Institute of Technology, Pasadena, California 91125

(Received 9 December 1986; accepted 11 February 1987)

This paper, the first in a series of three papers, gives a detailed account of our studies on picosecond photofragment spectroscopy. The unimolecular reaction NCNO→CN + NO is examined in detail here. Microcanonical state-to-state rates are measured in molecular beams at different energies in the reagent NCNO using pump–probe techniques: one picosecond pulse initiates the reaction from an initial (v,J) state and a second pulse, delayed in time, monitors the CN radical product in a specific rovibrational state, or the reagent NCNO (transient absorption). The threshold energy for reaction is determined to be 17 083 cm^{-1} (bond energy = 48.8 kcal/mol). Measured rates are found to be sharply dependent on the total energy of the reagent, but independent of the rotational quantum state of product CN. Results of transient absorption measurements are used to argue that the ground state potential energy surface dominates the reaction in the range of excess energies studied. The energy dependence of the rates, $k_{MC}(E)$, is compared with that predicted by statistical theories. Both standard RRKM (tight transition state) and phase space theory (loose transition state) fail to reproduce the data over the full range of energies studied, even though nascent product state distributions are known to be in accord with PST at these energies. Furthermore, $k_{MC}(E)$ is not a strictly monotonically increasing function of energy but exhibits some structure which cannot be explained by simple statistical theories. We advance some explanations for this structure and deviations from statistical theories.

I. INTRODUCTION

In preliminary publications from this laboratory, we have reported on the technique of pico-[1] and femtosecond[2] photofragment spectroscopy and its application to the measurement of absolute rates of different classes of reactions. In a series of forthcoming papers we present detailed accounts of these studies, focusing on the following reactions in this set:

(I) Predissociation of a stable molecule

$$NCNO \rightarrow CN + NO .$$

(II) Local-mode overtone-initiated predissociation[3]

$$H_2O_2(v_{OH} = 5) \rightarrow 2OH .$$

(III) Predissociation of van der Waals clusters[4]

$$\text{phenol–benzene} \rightarrow \text{phenol} + \text{benzene} ,$$
$$\text{cresol–benzene} \rightarrow \text{cresol} + \text{benzene} .$$

In these experiments, two picosecond (or femtosecond) pulses are overlapped spatially and temporally in a seeded supersonic molecular beam (or in a low-pressure gas). The first pulse initiates the reaction from an initial state $(v,J)_i$ and the second pulse, delayed in time, probes the population of nascent products in a specific final vibrational/rotational state $(v,J)_f$, or monitors the evolution of the initial state of the reagent. In the former case, the state-to-state rate constant $(k_{i\rightarrow f})$ is measured with picosecond or subpicosecond time resolution. Product state distributions (PSD) may also be obtained by comparing the population in different final states at delay times much longer than the lifetime of the initial state. Information on alignment and correlation of angular momenta can also be deduced from studies where the polarization of the pump pulse relative to the probe pulse is varied.

The systems we have studied so far each possess some features that merit discussion individually. In NCNO, the oscillator strength is carried by a bound, excited electronic state. Reaction is preceded by energy redistribution to a lower electronic state, presumably because the density of vibrational states is large for the lower state at the energies of interest. In H_2O_2, an overtone of the OH stretch is excited directly on the ground-state surface and the mixing with other internal degrees of freedom is an important component of the dynamics of bond dissociation. The van der Waals' system has elements common to the other two. The vibrational densities are large, yet there is a large disparity between the frequencies of the complex modes and those of the internal modes of the uncomplexed molecules. One may expect separability of the two sets of modes, which would lead to nonstatistical effects in a large system. Studies on these model systems will improve our understanding of the domain of validity of the assumptions commonly used to describe unimolecular reactions.

A reaction may be considered fully characterized when the multidimensional potential energy surface (PES) governing the motions of the constituent atoms is exactly known. Product angular and translational energy distribu-

[a] Present address: Dept. of Chemistry, Wesleyan University, Middletown, CT 06547.
[b] Contribution No. 7513.

 0021-9606/87/130077-20$02.10

tions measured in crossed molecular beams[5] offer important experimental data that can be used to test a model PES. Unimolecular reactions, or half-collisions, constitute a special subset of the infinite number of fragment internal energy and impact parameter combinations possible in the reverse reaction, a bimolecular scattering experiment. The measurable quantities in this simpler case are product internal and external (translation) energy distributions as well as absolute rates. Consider the typical unimolecular reaction from state α to the final state (β,γ):

$$A^*(v_\alpha,J_\alpha) \overset{k_{\alpha\to(\beta,\gamma)}}{\rightarrow} B(v_\beta,J_\beta;b) + C(v_\gamma,J_\gamma;b) \; .$$

Several parameters may be defined—the rate of disappearance of A ($K_\alpha \equiv \Sigma_{\beta,\gamma}\, k_{\alpha\to(\beta,\gamma)}$), the rate of formation of B or C and the impact parameter b. The state-to-state rate constant is the characteristic time constant for the appearance of products B or C in specific final states. The temporal behavior of A, B, or C can be measured in principle, b cannot be directly measured, but may be inferred from the distribution in different final states. K_α, the absolute reaction rate, cannot be derived from PSDs since the ratio of nascent population in different product states is simply the ratio of the state-to-state rates, $k_{\alpha\to(\beta,\gamma)}$, of dissociation into those channels.

The measurements of rates and PSDs yield different information relevant to the dynamics. PSDs contribute information on the distribution of impact parameters that include effects of long range interactions (dispersion forces and electron correlation). These measurements are made after the entire ensemble has reacted and involves time delays of several tens of nanoseconds between initiation and probing. In rate measurements, the time evolution of the ensemble is of primary interest; energy redistribution and early time dynamics leave their signature on the form of the transient. The hope here is to be able to view the dynamics at early times and to compare rate measurements with predictions of statistical theories such as RRKM, phase space theory (PST), or the statistical adiabatic channel model (SACM). The combination of time resolution and molecular beams makes it possible to measure directly the rates (and PSDs) of an ensemble which is essentially microcanonical, with specified energy and angular momentum. This affords a stringent test of the theories of energy redistribution and unimolecular dissociation.

This first paper (I) in the series presents measurements of the state-to-state reaction rates of the unimolecular dissociation of nitrosyl cyanide (NCNO) to nitric oxide (NO) and the cyanogen radical (CN). The PSDs for this reaction have been studied in a complete series of experiments by Wittig and co-workers[6] and found to be in agreement with PST. Our experiments reported here are performed in a supersonic beam to obtain initial states with a narrow spread in energy and angular momentum, in contrast to the previously reported work[1(c)] performed in a low pressure, ambient temperature bulb or in an effusive beam. By continuously and independently varying the pump and probe photon energies, we provide $k_{i\to f}$ for different initial total energy in the reagent and for different rotational states of the CN product. The functional dependence of the rates on energy shows a threshold for reaction which is the bond energy in the absence of an exit channel barrier. We find phase space theory (PST) and simple RRKM treatments inadequate for explaining the energy dependence of the rates, $k_{MC}(E)$, over the range of excess energies studied. We observe "structure" in $k_{MC}(E)$ and offer a number of possible explanations for these deviations, including the idea of *dynamical trapping* in the exit channel of the PES whose details are presently unknown.

This paper is structured as follows. The experimental section (Sec. II) contains a summary of our apparatus. The results and analysis section (Sec. III) give specific details of the different experiments done and their results, followed by a description of how the raw data was analyzed. The fourth section develops the theoretical background relevant to the discussion and includes a summary of statistical theories. The discussion (Sec. V) is broken up into several subsections. The first one (Sec. V A) presents some spectroscopic information on the reagent and the products. The next one addresses the significance of measuring the time dependence of product appearance in different channels (Sec. V B). The dependence of rates on the initial angular momentum is briefly discussed next. The influence of intramolecular energy redistribution on reaction rates is considered in the light of transient absorption and recent fluorescence measurements (Sec. V D). Calculated phase space theory and RRKM rates are compared with the experimental rates (Sec. V E), showing the inadequacy of both models in explaining the energy dependence. Possible explanations for the structure in $k(E)$ are also explored.

II. EXPERIMENTAL APPARATUS

A. Two-color picosecond laser system

It is necessary to have two independently tunable sources of high energy picosecond pulses in order to measure the excess energy dependence of the temporal behavior of a given product channel. A detailed description of the laser system is presented in paper II,[3] and only a summary is presented here. The 1064 nm output of an actively mode-locked Nd–YAG was frequency doubled by focusing in a KTP crystal. The 532 nm visible light ($\sim$800 mW) was divided into two beams of approximately equal intensity and each one used as the pump source for a synchronously pumped dye laser. The output wavelength of each dye laser was selected by an intracavity three-plate quartz birefringent filter. Both dye lasers used R6G in ethylene glycol as the gain medium. One of these (DL1) was used to generate light at 580–565 nm, while the other (DL2) was used to generate light at $\sim$610 nm. Typical pulses from each dye laser had Gaussian temporal profiles with a full-width at half-maximum (FWHM) value of $\sim$8 ps. The measured spectral bandwidth was approximately Gaussian with $\sim 3\ \mathrm{cm}^{-1}$ FWHM.

The pulses from the sync-pump lasers were amplified in two three-stage dye-amplifiers pumped by the doubled output of a Q-switched Nd–YAG laser operating at 20 Hz. A number of different dye solutions (R640, R610/R640, R610, KR620, R620/R590, and R590, all in methanol) were used to obtain proper amplification as the frequency of DL1 was changed. The visible output of amplified DL1 was

used as the pump with no further processing. The amplified output of DL2 was mixed with the 1064 nm fundamental of the DCR/2A in a KDP crystal to generate light at 388 nm and used to probe specific rotational states of the nascent ground-state CN radicals produced on dissociation.

The time delay between the two beams was set up in a Michelson interferometer. The pump beam (DL1) was directed through a fixed delay, while the probe beam (DL2) was directed through a variable delay consisting of a 2.5 in. hollow corner cube mounted on a stepper-motor driven translator (10.0 μ per step). The beams were combined in a dichroic mirror after which they were propagated collinearly and focused softly with a 1 m quartz lens into the expansion chamber. The focus was adjusted to be beyond the free jet, so that scatter and multiphoton processes could be minimized simultaneously.

The cross correlation of DL1 and DL2 after amplification was measured by generating the sum frequency[7] in a 1 cm KDP crystal. A typical cross correlation (Fig. 1) could be represented by a Gaussian envelop (FWHM$\approx$10 ps). The response functions for the transient absorption experiments described below were obtained by generating the difference frequency of the UV light (doubled DL1 or DL2) and the visible fundamental (DL1) in a KDP or $LiIO_3$ crystal. In this case the light generated had exactly the same frequency as the fundamental, but could be separated from it by using a spatial filter to give an essentially zero-background two beam signal. Figure 1 also shows typical cross correlations for this experiment when the tuning element in the laser was a two-plate birefringent filter. This configuration was used for some of the transient absorption studies described below.

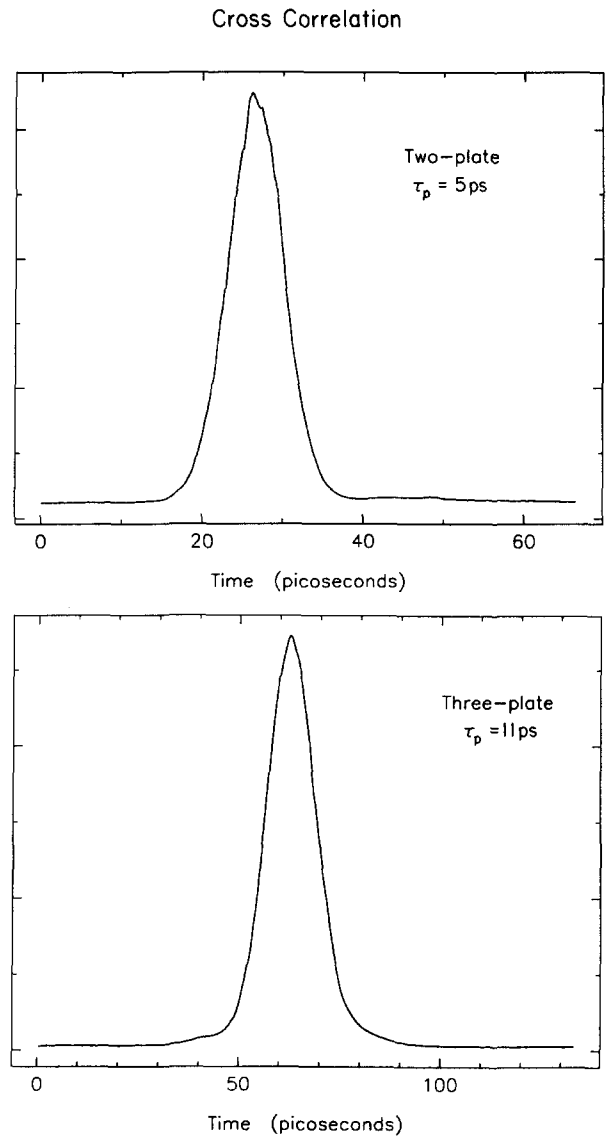

FIG. 1. Cross correlation of pump and probe lasers. The top figure was obtained by generating the difference frequency between the doubled output and the fundamental of DL1. A two-plate birefringent filter was used to reduce the temporal widths of the pulses. The lower trace was obtained by generating the sum frequency of DL1 and DL2. A three-plate birefringent filter was used in each sync-pump laser.

B. Molecular beam apparatus with LIF detection

A free jet expansion was used to eliminate internal energy in the parent NCNO molecule. The expansion chamber was pumped by two oil-diffusion pumps. The sample was introduced through a pulsed nozzle made of Kel-F, a perfluorinated, machinable plastic. The nozzle was operated at 20 Hz and triggered by the Q-switch of the YAG amplifier. The nominal aperture diameter d was 500 μ and the laser beams intersected the expansion 10 mm downstream from the nozzle, corresponding to $x/d \approx 20$. The results were not affected by decreasing d. Typical backing pressures of 1000 Torr He and nominal valve open-time of 100 μs resulted in an ambient pressure of 2×10^{-5} Torr at steady state. Short optical baffles were used on both input and output sides to reduce scattered light in the chamber.

Fluorescence was detected using a single $f/1$ quartz lens 2 inches in diameter which was adjusted to focus a point image defined by the laser beams and the axis of the expansion slightly beyond the detector. A UV sharp-cut filter (Corion LDS-370) and visible blocking filters (7-59 and interference-coated 7-54, Corning) were used to define the spectral window of detection. The detector was a high gain photomultiplier operated close to its maximum gain of 10^8. The output of the PMT was amplified and used as input to a variable gain boxcar integrator which was triggered off a fast photodiode illuminated by 532 nm light from the Q-switched laser. The gate for signal averaging was set to bias against laser scatter. The boxcar output was routed through a voltage to frequency converter and into a multichannel analyzer operated in the repetitive scaling mode. The channel step for the MCA was enslaved to a programmable stepper-motor controller which drives the optical delay translator. The data was averaged in the MCA and later transferred to a PDP 11/23 + minicomputer where it was analyzed and stored on floppy disks.

C. Sample preparation and handling

NCNO was prepared by the reaction of NOCl with AgCN according to the procedure of previous authors.[6,8] NOCl was prepared following a documented procedure.[9] Reagent grade chemicals were used in the syntheses without further purification. AgCN (Aldrich) was dried thoroughly under vacuum and cooled to -40 °C. NOCl was introduced

into the bulb containing AgCN and the gas–solid mixture was vigorously stirred. As the reaction proceeded, the vessel was kept cold with a bath of dry ice and acetone maintained below − 30 °C. After 15–20 min, the gaseous products were trapped out into a separate bulb immersed in liquid N_2. This procedure was repeated a number of times. The crude products which always contained a large amount of unreacted NOCl was purified by repeated bulb to bulb distillation from a hexane-liquid N_2 slush bath. Extreme care was taken during the synthesis as several reports of explosions have been made.[8]

A 22 *l* bulb was evacuated to ~100 mTorr and pure NCNO introduced to ~1 Torr. The bulb was then pressurized to 1000 Torr with He and connected to the input line for the pulsed nozzle. The bulb was refilled with pure He every 2 h, during which time the pressure in it dropped to ~800 Torr. This procedure could be repeated 20 times before the total signal level would start to affect the quality of the data. At that point the bulb was evacuated and fresh sample introduced. Except where specifically stated, this was our operating condition for all transients recorded.

The experiments to elucidate initial J dependence of dissociation rates were done similarly, with the following differences. A much smaller bulb (5*l*) was used and N_2 was the carrier gas employed. The bulb was pressurized to 100 Torr and the drop in pressure over 1.5 h was ~10 Torr. The sample delivery manifold was checked carefully against leaks to the atmosphere. These expansions are referred to later as *warm*.

III. RESULTS AND DATA ANALYSIS

Several different types of experiments were undertaken and a short description of each type is given below, with the results obtained in each case. The molecular transient response for a combination of pump and probe wavelength was obtained by varying the delay between the pulses. Care was taken to ensure that the range of the delay was $\gtrsim 4\tau$, where τ is the characteristic constant of a single exponential fit to the data. This was possible for all cases except at threshold, where τ was longer than 1 ns.

A. Product rotational state dependence

In this set of experiments, the pump laser (DL1) was tuned to a known absorption band of the parent molecule.[6] The probe laser (DL2) was tuned to a wavelength such that the sum frequency obtained after mixing with the 1064 nm was resonant with a specific transition in the R branch of the $\Delta v = 0$ band of the $B\,^2\Sigma^+ \leftarrow X\,^2\Sigma^+$ electronic transition of CN.[10] With the pump laser frequency fixed, the wavelength of the probe laser was tuned to various resonances in the R branch corresponding to different rotational levels (N'') of ground state CN. A series of transients corresponding to different N'' and a fixed pump wavelength showed characteristic risetimes which were identical within experimental error. This was observed for several different pump energies in the range of excess energies covered in this study.

B. Excess energy dependence

These experiments were similar in concept to the ones described above. The pump laser was tuned to a vibronic transition in the $S_1 \leftarrow S_0$ absorption band. The probe laser was tuned to monitor a single N'' state in the ground state of CN, typically the one with maximum probability for population on dissociation of NCNO. In this set, the probe laser remained fixed for the most part, while the pump laser was tuned through the absorption spectrum.

The dissociation rate of NCNO, as manifested by the appearance rate of the fragment CN, as a function of the excess energy in the parent was measured from 5853 to 5630 Å. The threshold for reaction derived from this data set is 17 083 cm^{-1}, in excellent agreement with the reported value of 17 085 cm^{-1}.[6] In the range of energies studied, the characteristic constants varied from $\geqslant$2.0 ns at threshold to 10.0 ps at 690 cm^{-1}. Typical transients are shown in Fig. 2 and the fitted rate constants are plotted as a function of excess energy in Fig. 3. A study of the signal intensity as a function of the pump laser power showing linear dependence is presented in Fig. 4. The signal was also found to vary linearly with the intensity of the probe laser.

C. Total angular momentum dependence

In order to investigate the effect of parent rotation on the rate of decomposition, we changed the expansion conditions. A *warm* expansion would leave significant population in higher J states of the parent. The pump wavelength was held fixed at 5846 Å which lies in the middle of an unstructured region of S_1 absorption. The probe was tuned for different N'', as described in Sec. III A, and the responses measured are shown in Fig. 5. These rates show a marked dependence on N'', the effect being particularly striking for the highest N'''s, which show a biexponential temporal behavior.

D. Transient absorption

This set of experiments was designed to probe the bound parent molecule. As before, DL1 was tuned to a resonance in S_1. The amplified light of DL1 was frequency doubled to generate 285 nm, which was then used as the probe. The UV probe may also be obtained by frequency doubling the output of DL2. Fluorescence dependent on both fields was observed and identified as spontaneous emission from the $B\,^2\Sigma$ state of CN using appropriate cutoff filters. The measured lifetime of this fluorescence was found to be 56 ns, which is identical to that of the fluorescence observed using a probe resonant with the CN $B \leftarrow X$ transition.[10] The signal was linearly dependent on the intensity of both fields. In this scheme, molecules absorbing photons from both pump and probe fields dissociate to the electronically excited B state of CN (Fig. 6).

The transient absorption of the parent was measured at a number of different energies above and below the threshold for dissociation. For excitation below threshold, the pump laser was tuned to a weak S_1 resonance at 5912 Å.[11] The

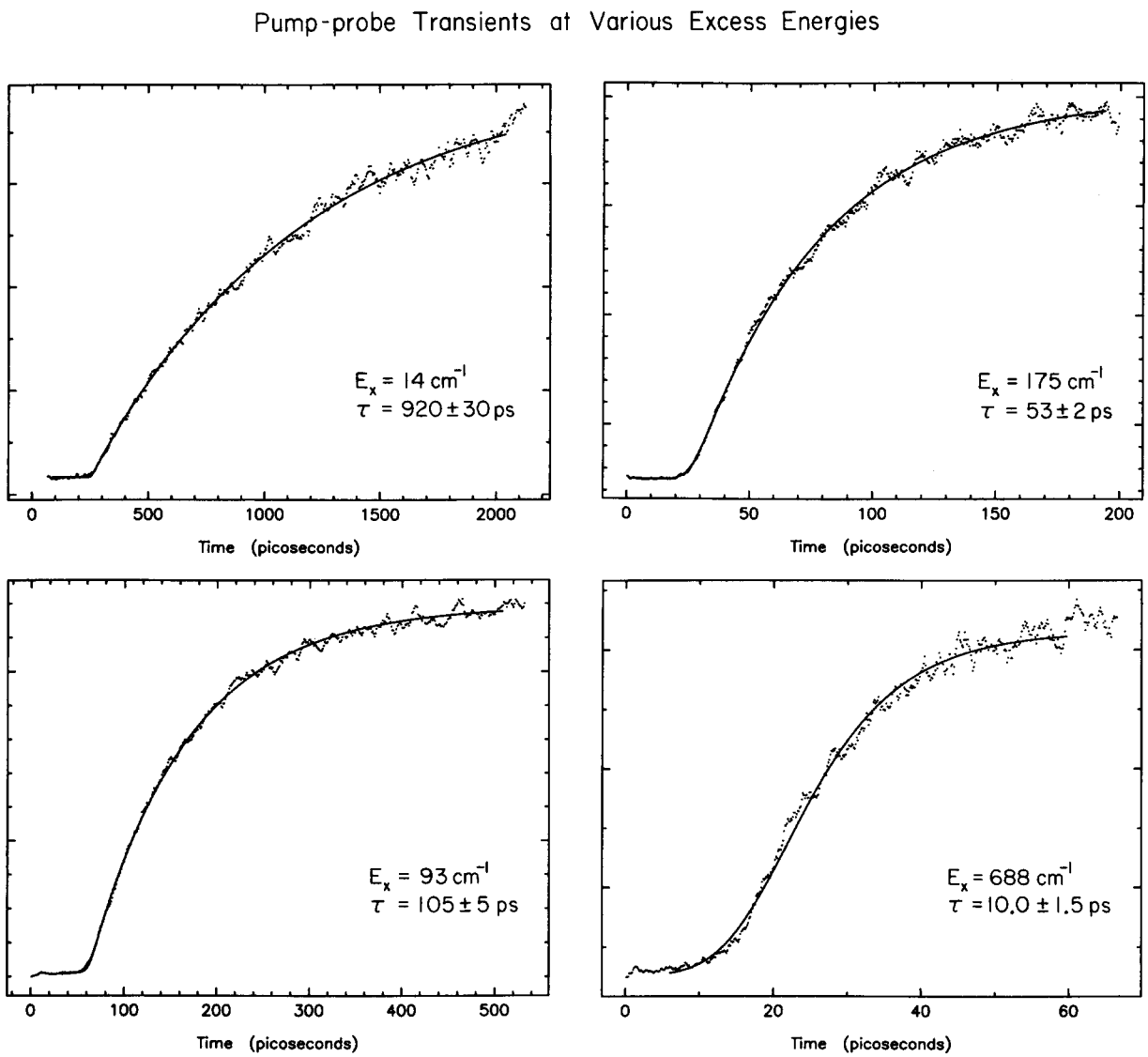

FIG. 2. Typical transients observed at different pump energies. The solid lines are our best fit of the data to single exponential buildup (see the text). The same applies to other related figures.

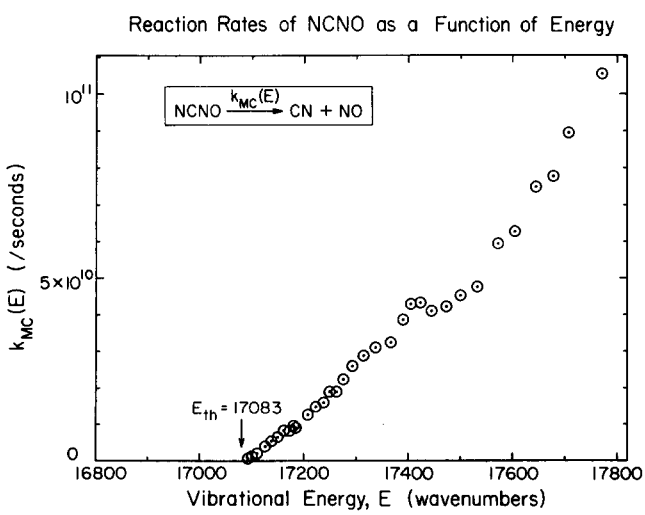

FIG. 3. The excess energy dependence of measured microcanonical rates from 5853 to 5630 Å. Included in this data are the rates measured for different N'' states of CN. As mentioned in the text, different N'' show the same rate when measured in a cold expansion.

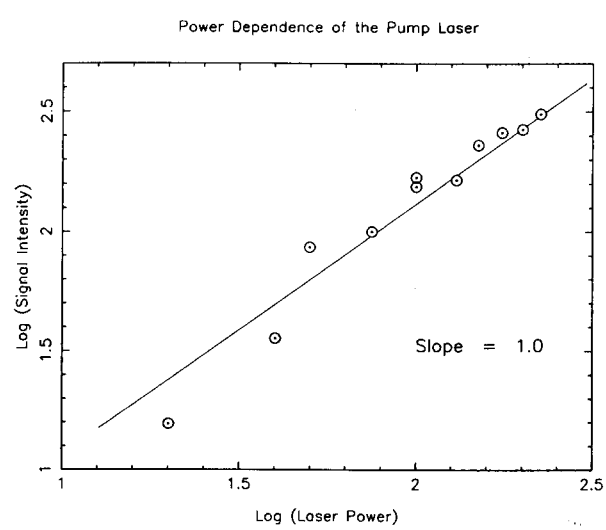

FIG. 4. Observed signal intensity as a function of the intensity of the pump laser. The background was obtained by measuring the signal at large negative time and subtracting it from the signal at large positive time.

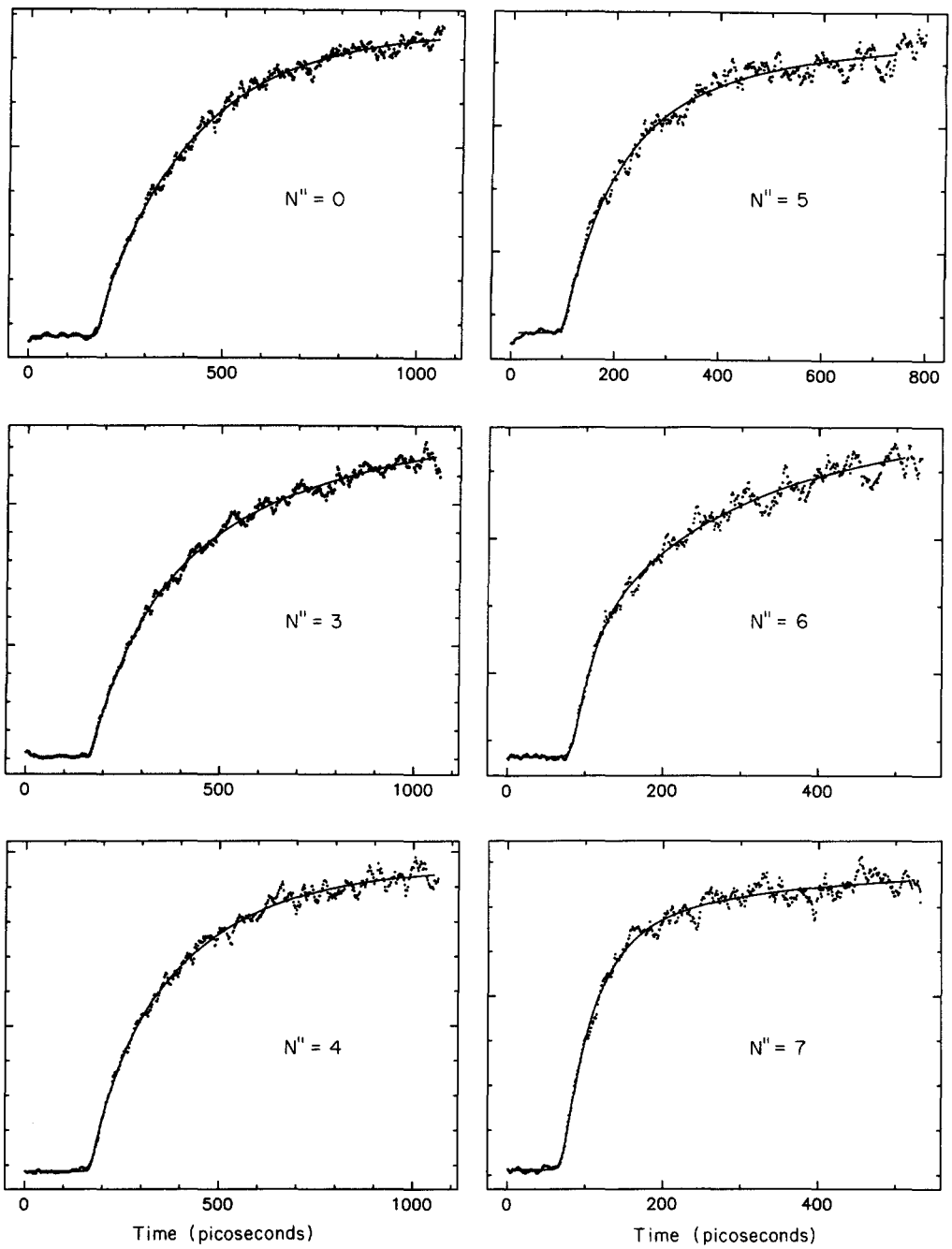

FIG. 5. Transients observed while probing different CN(N'') with pump frequency fixed at 5845 Å. These experiments were done on the *warm* expansion (see the text).

measured response showed an instantaneous rise and no subsequent decay on our time scale. At all excess energies above threshold, the measured decays were exponentials, with the time constant equal to that of the corresponding rise of CN at the same pump energy. Typical transients at different energies are presented in Fig. 7.

E. Data analysis

The system response function was approximately Gaussian. The standard nonlinear least-squares analysis based on the Marquardt algorithm[12] was used to fit the cross correlations to this functional form. Typical pulse FWHM values were in the range 9.5 to 11.5 ps.

The pulse width obtained from a fit of the cross correlation to a Gaussian form was used to derive accurate rate constants from the molecular responses measured in the experiments described in Secs. III A–III C. Although the cross correlation of the two visible beams is not the true system response, the 388 nm radiation used in these experiments appears to have the same temporal profile as that of the fundamental visible used to generate it. A simple argument supporting this observation is that the temporal fluctu-

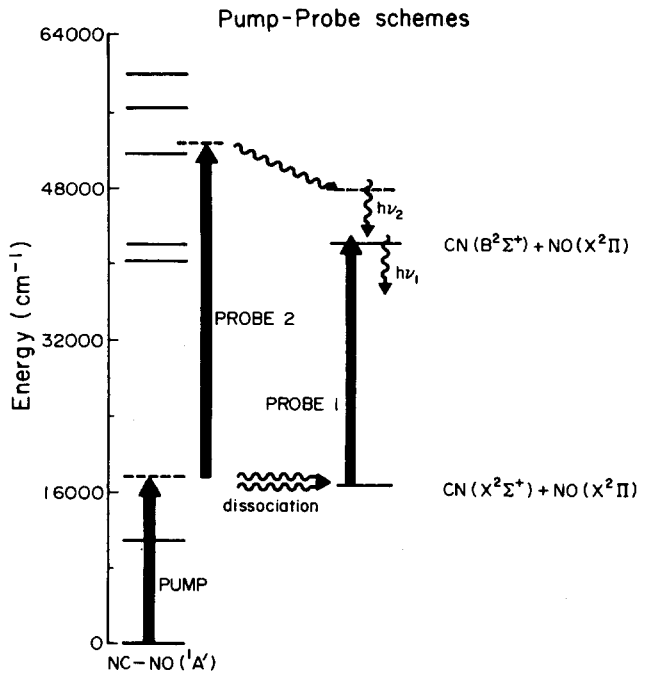

FIG. 6. Experimental schemes for transient absorption and CN state selected detection. Pump and probe wavelengths are independently tunable. PROBE 1 corresponds to resonant excitation of specific rotational states of product CN. PROBE 2 is absorbed by the bound molecule; the highly excited NCNO dissociates into electronically excited CN, and the spontaneous fluorescence is detected.

ations in the intensity of the ~3 ns, 1064 nm beam from the Q-switched YAG should be negligible over 10 ps, the time range of interest. The measured cross-correlation functions were used to deconvolute the transient decays described in Sec. III D. The fitted decay lifetimes were found to be the same as those obtained by deconvoluting the transients with a Gaussian pulse simulating the cross correlation.

The data reduction code was also based on the same algorithm and set up for the analysis of fluorescence decays. As shown in the Appendix, the convolution of a pulse with an exponential rise has the same mathematical form as the convolution of the integral of the pulse with an exponential decay having the same time constant. We used the second approach to deconvolute our data to derive the reported dissociation rates.

The transients presented in the figures were all smoothed using a three-point averaging algorithm.[13] Since the exponential constants were typically 100 channels, averaging has little effect on the derived rate constants. Reduced χ^2 values obtained with statistical weighting were in the range 2.0 to 5.0. The weighted residuals showed that the nonrandom noise distribution responsible for these large values had high frequency components that may be due to the mode quality of the pulsed YAG amplifier and imperfect alignment of the interferometer.

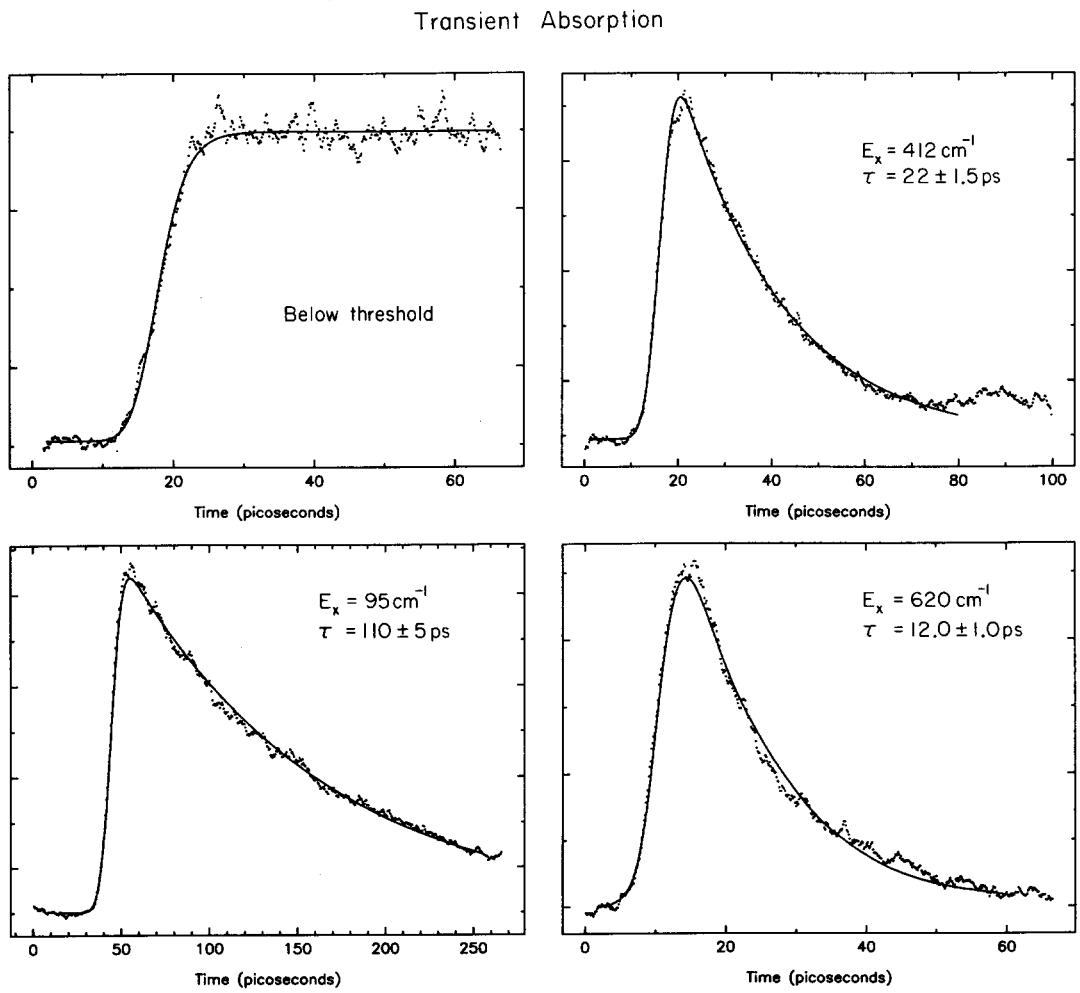

FIG. 7. Transient absorption signals measured at different pump energies. Note the agreement with results in Fig. 2 for $E_x = 95\ \text{cm}^{-1}$. The same agreement was found at other excess energies studied.

IV. THEORY

A. Kinetic model

A quasibound or metastable state has a wave function which can be represented in a low-order approximation by a superposition of a bound state and continuum wave functions.[14] The bound states form a basis in a local sense, i.e., if the system is restricted to a small volume in configuration space. It is well known that an isolated level coupled to a continuum can be represented quantum mechanically as a state having a complex energy.[15] Population in these states, if observable, would decay exponentially with a time constant proportional to Γ, the effective coupling constant. A polyatomic molecule dissociating into two fragments can be formally represented in the same way. The true bound states of the parent molecule may be used to construct an approximate basis set. Each set of bound state quantum numbers of the fragments has an associated translational energy continuum to which the bound states of the parent polyatomic are coupled. Thus so-called *state-to-state* rates of an unimolecular dissociation process are simply measures of the coupling strength of an approximate molecular state to each continuum channel.

The obvious kinetic scheme for the dissociation of a polyatomic molecule A into two fragments B and C is shown in Fig. 8. The sets $\{v_i,J_i,\tau_i\}_X$ designate the vibrational (v_i) and rotational (J_i,τ_i) quantum numbers of the molecule X and identify the initial state i. Population in the ith state of X at time t is abbreviated to $[X_i(t)]$ below. The solutions to the three simultaneous linear first-order differential equations describing the temporal behavior of each molecule are readily obtained. If the initial conditions are that only $[A_\alpha(0)]$ is nonzero,

$$[A_\alpha(t)] = [A_\alpha(0)]e^{-K_\alpha t}, \tag{1}$$

$$[B_\beta(t)] = [A_\alpha(0)] \sum_\gamma \frac{k_{\alpha\to(\beta,\gamma)}}{K_\alpha}[1-e^{-K_\alpha t}], \tag{2}$$

$$[C_\gamma(t)] = [A_\alpha(0)] \sum_\beta \frac{k_{\alpha\to(\beta,\gamma)}}{K_\alpha}[1-e^{-K_\alpha t}], \tag{3}$$

where $K_\alpha = \Sigma_{\beta,\gamma}\, k_{\alpha\to(\beta,\gamma)}$. The sums in Eqs. (2) and (3) are to account for the correct counting of channels for, say, fragment B in a quantum state β with all possible concomitant states γ of fragment C. The observed time dependence will be exponential, a decay for A and buildup for B or C, with time constant equal to the *total rate* of depopulation of the initial state. The probability of products appearing in channel (B_β,C_γ) is $k_{\alpha\to(\beta,\gamma)}/K_\alpha$. Therefore, analysis of product state distributions must be used with measurements of absolute rates to derive estimates of $k_{\alpha\to(\beta,\gamma)}$. Furthermore, PSDs cannot provide absolute rates (K_α) since they only give ratios of $k_{\alpha\to(\beta,\gamma)}/K_\alpha$.

This description of a unimolecular reaction is useful for comparison between theory and experiment only if the nature of the initial state(s) and their coupling(s) to the translational continua are known. The true molecular basis of the bound molecule cannot be exactly specified since all the interactions between the internal degrees of freedom are typically not known. In practice, additional simplifying assumptions that allow one to predict $k_{\alpha\to(\beta,\gamma)}$, K_α and other quantities of interest as functions of globally conserved quantities E and J are made. One of these, the statistical approximation, is discussed briefly.

B. Statistical models for microcanonical rates

A proper statistical treatment of rates conserves all constants of motion and weights all degeneracies equally. For a typical potential energy surface with a single saddle point (Fig. 9) representing the unimolecular reaction $A\to B+C$, the classical microcanonical rate is proportional to the flux of points through a hypothetical surface S_m in phase space. If S_m is drawn such that a given trajectory will intersect it at most once, the rate is given by[16,17]

$$k = \frac{1}{h^n\rho^{(n)}(E)} \int dp \int dq\, \delta[E-H(p,q)] \times \delta[f_0(q)]\left(\frac{\partial f_0}{\partial q}\cdot\frac{p}{\mu}\right) G_0\left[\frac{\partial f_0}{\partial q}\cdot p\right].$$

q and p are generalized coordinates and momenta, each integral is n-dimensional, E is the total energy, $H(p,q)$ is the n-dimensional Hamiltonian, $G_0(x)$ is the unit step function, $\rho^{(n)}(E)$ is the density of states in the vicinity of the well respresenting A, and $f_0=0$ defines the $(n-1)$-dimensional dividing surface, S_m. $\delta[E-H(p,q)]$ in the integral specifies a microcanonical (MC) ensemble, $\delta(f_0)$ restricts the integral over coordinate dimensions to S_m, and the last two factors constitute the forward flux from A to products through

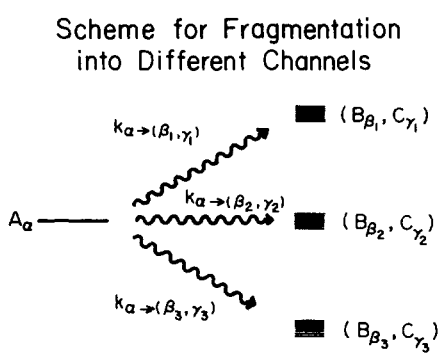

FIG. 8. Kinetic model for dissociation into various fragment channels identified by quantum numbers.

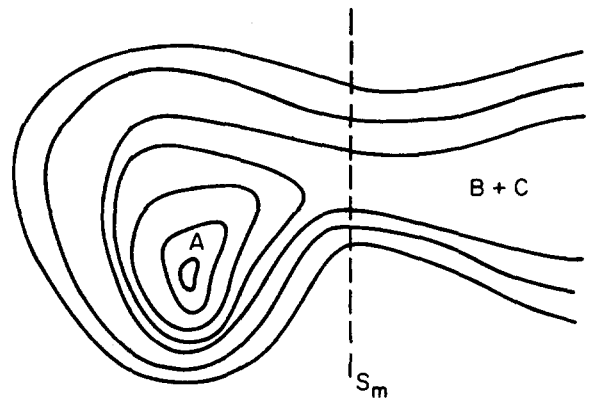

FIG. 9. A two-dimensional contour representation of a typical potential energy surface for unimolecular dissociation of A into B and C.

it. The integral reduces to the microcanonical partition function of the system restricted to the dividing surface which is the usual juncture for introducing quantization.[16,17] The MC partition function is the total number of bound states with energy less than E,$N(E)$. Using a superscript † to emphasize that the relevant integral has one less degree of freedom, the rate assumes the familiar expression associated with RRKM theory[16]:

$$k_{\mathrm{MC}}(E) = \frac{N^{\dagger}(E^{\dagger})}{h\rho(E)}. \tag{4}$$

An application of this formula requires knowledge of the shape and position of the dividing surface as well as ρ. How correct a calculation of the rate constant is will be determined by how accurately S_m is described and how well $\rho(E)$ is assessed. The choice of S_m must satisfy a minimum flux ($N^{\dagger}$) criterion,[18] but its shape cannot be completely specified without detailed knowledge of the potential energy surface (PES). Standard methods of approximating $N^{\dagger}$ without recourse to the PES are described below.

1. RRKM theory

The zero-order approach is to model S_m by a surface perpendicular to q, the coordinate that best describes the bond being broken, and similar in shape to one drawn through the local minimum of the potential corresponding to A, and also perpendicular to q. This approximation, known as *standard* RRKM, is clearly an idealized case and will be good if the true S_m lies close to the equilibrium position of the reactants. In more familiar terms, S_m represents a fictitious molecule (*critical configuration* or *transition state*) with one less degree of freedom than the reactant. This lost degree is the reaction coordinate and is used to parametrize the extent of reaction in an intuitive sense. A standard RRKM calculation thus assumes a transition state whose vibrational frequencies and rotational constants are the same as the corresponding ones in the reactant. In the literature, this is referred to as a *tight* transition state.

2. Phase-space theory

For transition states of infinite looseness, yet another idealized case has been used to estimate $N^{\dagger}$ with explicit conservation of angular momentum. In this model,[19] S_m is placed at the local maximum of an effective potential, V_{eff}, obtained from the sum of a long range attraction, $V_b(r)$, and centrifugal repulsion due to orbital motion of the separating particles. Energy conservation imposes an upper limit on the orbital momentum quantum number. For a tetraatomic molecule (A) dissociating into two diatomic fragments (B and C), the conservation laws are

$$\mathbf{J} = \mathbf{J}_{\mathrm{A}} = \mathbf{J}_{\mathrm{B}} + \mathbf{J}_{\mathrm{C}} + \mathbf{l}, \tag{5}$$

$$E_{\mathrm{avail}} = E - \max\{V_{\mathrm{eff}}(r)\} \geqslant \sum_{n=\mathrm{B,C}} E_n(\mathrm{vib}) + E_n(\mathrm{rot}), \tag{6}$$

$$V_{\mathrm{eff}}(r) = V_b(r) + \frac{\hbar^2 l(l+1)}{\mu r^2}. \tag{7}$$

E is the energy in the parent and $V_b(r)$ is a one-parameter representation of the potential energy along the bond dissociation coordinate. The dissociation energy E_0 is $V_b(\infty)$. Note that E_0 includes the zero point energies of the reactant and products. $\mathbf{J}_{\mathrm{A}}$ is the total angular momentum of the parent, $\mathbf{J}_{\mathrm{B}}$ and $\mathbf{J}_{\mathrm{C}}$ the total angular momentum of B and C, respectively, and $\mathbf{l}$ the angular momentum of the relative motion of the separating fragments. E_n (vib) and E_n (rot) are the vibrational and rotational energies of the fragment n. μ is the reduced mass and the second term in the right-hand side of Eq. (7) is the centrifugal potential. $E - E_0$ is the total energy available for product translation and internal motion at large distances. E_{avail} is this energy minus the centrifugal barrier to recombination (the reverse reaction) for each value of l. The barrier energy appears exclusively as translational energy in the separated products. Generally, V_b is approximated by the attractive part of the Lennard-Jones 6-12 potential. $N^{\dagger}$ is then obtained by counting all possible combinations of product quantum numbers satisfying energy and angular momentum conservation:

$$N^{\dagger}(E - E_0) = \sum_{v_n} \sum_{J_{\mathrm{B}},J_{\mathrm{C}},l} \kappa. \tag{8}$$

The parameter κ is a measure of the contribution of a combination of quantum numbers to the reaction rate and should be a constant for a proper statistical theory. It may be regarded as the microscopic transmission coefficient and is generally chosen to be unity. The sum in Eq. (8) is over all allowed J_{B},J_{C},l and vibrational states, v_n. It is convenient to define J', an intermediate quantum number corresponding to the sum of $\mathbf{J}_{\mathrm{B}}$ and $\mathbf{J}_{\mathrm{C}}$, in performing the calculation of $N^{\dagger}$. The conservation of angular momentum imposes the following restrictions on J' and l:

$$|J_{\mathrm{B}} - J_{\mathrm{C}}| \leqslant J' \leqslant J_{\mathrm{B}} + J_{\mathrm{C}},$$
$$|J' - l| \leqslant J \leqslant J' + l.$$

It should be noted that the degeneracies of J_{B},J_{C}, and l have been included in the sum, but they do not appear explicitly in Eq. (8).[20]

3. Refined models

Standard RRKM and PST represent two extreme cases. A number of modifications have been proposed to better mimic physical situations which most probably lie between these cases. The frequencies and rotational constants of the transition state can be modified following intuitive semiquantitative prescriptions.[21] Another variation (SACM) proposes a method for parametrizing molecular quantum numbers by the reaction coordinate and examining each such adiabatic channel to determine whether it is energetically accessible at all points between reactants and products.[22] PST has been criticized because it allows free rotation of the fragments within the transition state complex. A method (SSE)[6] for calculating PSDs that treats vibrations and rotations somewhat differently has been recently proposed and applied to the dissociation of NCNO at energies where product vibrations are excited and PST overestimates the extent of rotational excitation in the fragments. Classical trajectory calculations[23] offer a means of avoiding the statistical assumptions but require explicit knowledge of the PES.

The minimum flux criterion mentioned is derived from treating k_{MC} variationally. Several treatments have formalized this approach as microcanonical variational transition state theory.[24] A recent treatment of the dissociation of small polyatomic molecules involving transition states of arbitrary looseness uses canonical variables and Monte Carlo techniques for numerically estimating the multidimensional integrals in Eq. (4).[25] All of these methods presume a model of the PES which may be altered to obtain better agreement with experimental observations. We leave applications of these more elaborate models for future work.

V. DISCUSSION

A. Preliminary considerations

Before embarking on a detailed analysis of our results, we summarize the spectroscopy of NCNO and the fragment radicals CN and NO in this section. We also address the issues related to the selectivity of these experiments, namely, how well do we know our initial and final states.

1. Spectroscopy of parent and fragment molecules

NCNO has been thoroughly studied by microwave,[26] infrared,[27] and visible[28] spectroscopy. Studies by Wittig and co-workers on jet-cooled NCNO has provided rich information on the spectra.[28] Molecular constants for both ground state and excited state NCNO taken from the current literature are listed in Table I. The molecule is bent and planar in the ground state and has C_s point group symmetry. In the first excited singlet state ($n\pi^*$), the molecule is also planar and bent. Strong perturbations in the spectrum have been attributed to extensive mixing with the ground singlet state promoted by the bending modes. Near the S_1 origin, the rotational structure has been resolved and the band assigned[28] as a C-type transition, i.e., the transition moment is perpendicular to the molecular plane and parallel to the c axis of inertia.[29] At higher energies, vibronically induced A/B-type transitions to nontotally symmetric bands are observed.

TABLE I. Spectroscopic parameters of NCNO, CN, and NO.

NCNO: Vibrational frequencies and rotational constants (Refs. 26–28) (cm^{-1})				
ν_1''	CN stretch (*terminal*)	2170	A''	2.71
ν_2''	NO stretch	1501	B''	0.18
ν_3''	CN stretch (*central*)	820	C''	0.16
ν_4''	CNO bend	216.5	A'	4.77
ν_5''	NCN bend	588.5	B'	0.16
ν_6''	out of plane bend	269.6	C'	0.16
	CN: Molecular constants (Ref. 32) (cm^{-1})			
$^2\Sigma$				
	ν	2068.7		
	B_v	1.889 8		
	γ	0.007 25 spin–rotation constant		
	NO: Molecular constants (Ref. 32) (cm^{-1})			
$^2\Pi_{\frac{1}{2}}$				
	ν	1904.03		
	B_v	1.672		
$^2\Pi_{\frac{3}{2}}$				
	ΔE_{so}	119.62 spin–orbit splitting		
	ν	1903.68		
	B_v	1.720		

Overtones and combinations of the ν_4 bending mode are considerably broader than other transitions at comparable energies, indicating its role as a promoting mode for S_1–S_0 mixing.[28] Similar effects have been observed in the absorption spectrum of HNO[30] and likewise attributed to perturbations between the two lowest states. A sharp onset for the production of CN radicals occurs at 17 085 cm^{-1}. The S_1 absorption spectrum in this energy region shows structure reminiscent of C-type bands, but the rotational substructure of these bands cannot be resolved with laser linewidths of 0.04 cm^{-1}. This must be due to perturbations of the levels, since the measured dissociation rate at threshold ($\sim 10^8\ s^{-1}$) implies homogeneous widths $\sim 0.001\ cm^{-1}$. Fluorescence measurements have been recently made on expansion cooled NCNO (see Sec. V D) and estimates of the radiative lifetime (20 μs) can be made for these nitroso compounds.

The fragment CN is a typical Hund's case (b) diatomic.[29] The ground state is a $^2\Sigma$ state and the angular momentum without spin (N) is an approximate quantum number. N is the sum of nuclear rotational angular momentum (R) and the electronic orbital angular momentum (Λ), and is coupled weakly to the electron spin. The appropriate energy expressions[31] are given below and an energy level diagram showing some of the rotational levels is presented in Fig. 10:

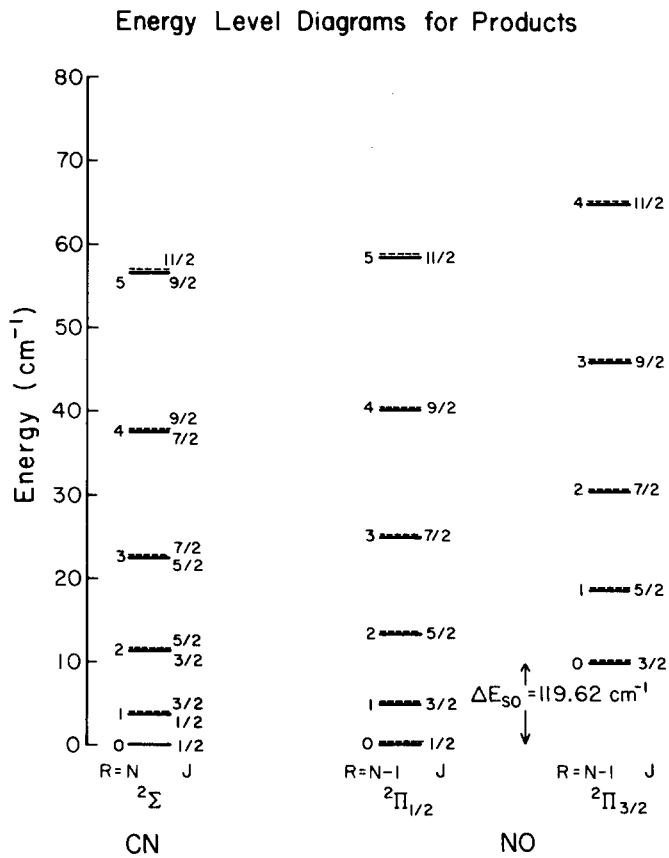

FIG. 10. Energy level diagram showing rotational states of CN and NO. The numbers on the left of each set of levels (R) identify it with the nuclear rotational angular momentum. The labels to the right correspond to the *total* angular momentum J. Note that the spin–orbit splitting of NO is not represented to scale. The spin–rotation and λ-doublet splittings (dashed levels) are exaggerated for clarity. For CN, N is a good quantum number, while J is the quantum number for NO.

$$F_1(N) = B_v N(N+1) + \tfrac{1}{2}\gamma N ,$$
$$F_2(N) = B_v N(N+1) - \tfrac{1}{2}\gamma (N+1) .$$

The total angular momentum J is given by $N \pm \frac{1}{2}$ for the states F_1 and F_2, respectively. B_v is the rotational constant in a particular vibrational state and γ is the spin–rotation coupling constant.

The fragment NO is a typical Hund's case (a) molecule. The ground state is $^2\Pi$ and nonnegligible spin–orbit coupling breaks the degeneracy due to the nonzero projection of the electronic spin angular momentum on the internuclear axis. The total angular momentum (J) is the sum of the rotational angular momentum and the electronic angular momentum including spin. Each level is doubly degenerate, corresponding to the two possible ways of electron motion about the figure axis. For high values of J, this degeneracy is also removed (λ-doubling). The appropriate energy expressions for the $^2\Pi_{1/2}$ and $^2\Pi_{3/2}$ states are[31]

$$E_J(^2\Pi^{\pm}_{1/2}) = B_v^{(1/2)} J(J+1) \pm \xi_{1/2}(J) ,$$
$$E_J(^2\Pi^{\pm}_{3/2}) = B_v^{(3/2)} J(J+1) + \Delta E_{so} \pm \xi_{3/2}(J) .$$

The energy scale is referenced to the lowest rotational level ($J = 1/2$) of the $^2\Pi_{1/2}$ state. $\xi_{1/2}$ and $\xi_{3/2}$ are the J dependent corrections to the energy due to orbital–rotation (spin–uncoupling) interaction and are important only for high J. These terms are ignored in the discussion below. ΔE_{so} is the spin–orbit splitting which is the energy of the lowest rotational level ($J = 3/2$) of the $^2\Pi_{3/2}$ state. It is important to note that the energy in this case is determined primarily by J and not N, in contrast to CN. The spectroscopic constants are collected in Table I.

2. Resolution of initial and product states

The final distribution of internal energy in molecules in a free-jet expansion is generally described in terms of effective vibrational, rotational, and translational temperatures.[33] These values depend on the carrier gas used and are typically small, ~ 10 K for vibrational, ~ 5 K for rotational, and ~ 1 K for translational distributions. In NCNO, the smallest ground state vibrational fundamental is 216 cm^{-1} which has an occupation probability of 0.002 at 50 K. Thus vibrational energy in the parent may be ignored for cold expansions. On the other hand, the rotational constants are small and a significant fraction of the molecules lie in states with $J > 0$. Under similar expansion conditions Noble *et al.*[28] determined rotational temperatures of 2 K by resolving the rotational fine structure of the origin band. Their estimate of the average rotational quantum number is $J = 3$. On scanning the frequency of the probe laser at a number of fixed pump energies, we observed a sharp drop in signal intensity for probe frequencies greater than that required to detect CN fragments with the maximum rotational quantum number that is energetically allowed, as reported by Nadler *et al.*[6] This suggests that the spread of internal energies in NCNO in our expansion is also small and we assume that the terminal rotational temperature in our studies is also ~ 2 K.

The $S_1(^1A'') \leftarrow S_0(^1A')$ transition in NCNO is dipole allowed (orbitally forbidden[28]) having its moment parallel to the principal axis of largest moment of inertia (C-type). The approximate symmetric top selection rules (perpendicular-type transition) are

$$\Delta J = 0, \pm 1 \quad \Delta K = \pm 1 .$$

At excitation energies near dissociation threshold where mixing with another electronic state is believed to be extensive, the pure rotational quantum number is not a good one but the total angular momentum must be conserved. The reactive ensemble is essentially microcanonical with angular momentum $J = 3$ and energy equal to the sum of the photon energy and the rotational energy. The spectral bandwidth of the excitation laser is 3 cm^{-1} FWHM, which determines the spread in energy in the reactive ensemble.

The probe laser is tuned to a specific transition in the R branch ($\Delta N = +1$) of the $B \leftarrow X$ band of CN. This transition shows a bandhead in the P branch when the diatom is rotationally very excited. The R branch was chosen to avoid spectral overlap between transitions from different N'' levels at the higher excitation energies. The spectral bandwidth of the probe laser (3 cm^{-1}) is smaller than the spacing between adjacent peaks in this branch. Thus different N'' states of CN can be monitored quite cleanly, although the different spin–rotation states (F_1 and F_2) are not resolved. Since simultaneous measurements on NO were not made, the population of CN in a particular N'' state observed at any time is the sum over all open product channels having that value of CN(N'').

3. Electronic state correlation

The concept of a PES on which nuclear motion takes place is entrenched in the Born–Oppenheimer approximation. The terms in the complete Hamiltonian that are ignored in the approximate treatment result in small coupling terms between the zero-order eigenfunctions. The separability of nuclear and electronic coordinates implies that the electronic quantum numbers are conserved independently. For a system where the nuclei are constrained near their equilibrium configuration, this approximation is quite successful. On the other hand, one expects it to be inadequate for the quantitative description of a system which is undergoing dissociation into fragments that are very different from the parent molecule. Nevertheless, correlations between states with the same electronic quantum numbers may be used to obtain qualitative knowledge of the shape of the PES as the nuclei rearrange or separate during a chemical reaction.

For the case at hand, it is simplest to consider the reverse process, recombination of the radicals CN and NO, proceeding through a linear complex which then rearranges to the equilibrium structure of NCNO (Fig. 11). If spin–orbit interaction in NO were ignored, the ground state diatomics would combine to form a $^1\Pi$ and a $^3\Pi$ state in a linear NCNO. At the equilibrium geometry each doubly degenerate Π state also splits into two (A' and A'' in C_s). The singlet states are nondegenerate whereas the three spin components of the triplet states remain quasidegenerate. Similar arguments must be developed for all combinations of electronically excited states of CN and NO and correlated to electronic states of NCNO. The ordering of the electronic states

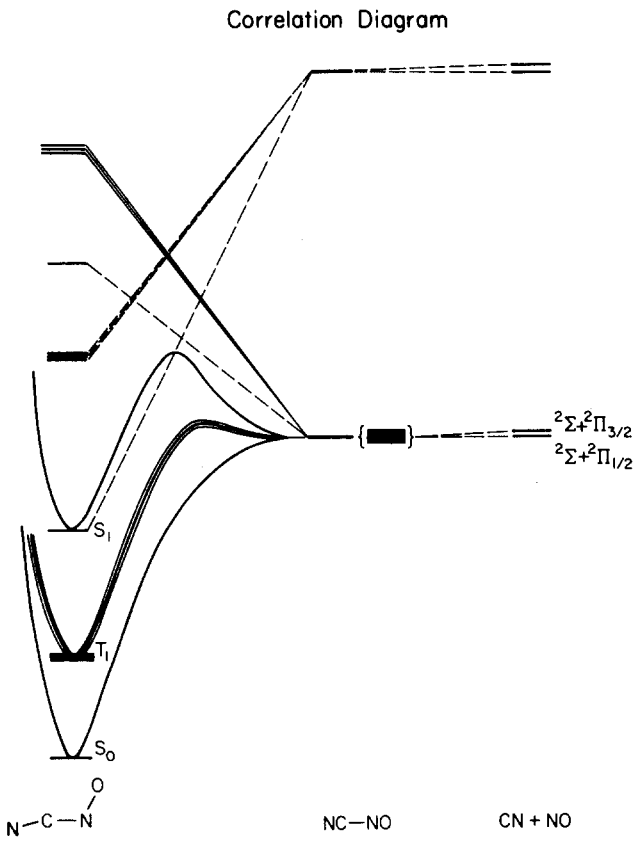

FIG. 11. Correlation diagram for the dissociation of NCNO. The leftmost column shows the order of energy levels in the parent molecule schematically. The far right column shows the energy of the products at infinite separation. The center column represents the molecule with the central CN bond greatly extended and the fragments arranged in a linear geometry.

by energy cannot be deduced without detailed calculations of its electronic structure. Recent calculations[34] show that the ground singlet and lowest triplet states are derived from ground state CN and NO, but the next most energetic singlet and triplet states are obtained from CN(X) and a highly excited configuration of NO. Topological constraints demand that these curves intersect the higher NCNO states correlating to CN(X) and NO(X). The pairs of states involved have the same symmetry and their interaction leads to an avoided crossing, which predicts a substantial barrier to dissociation from S_1 and T_2 to ground state CN and NO fragments.

B. Product rotational state dependence

As shown above for an isolated resonance coupled to a finite number of continua, the rise time observed in any channel is the absolute rate of depopulation of the resonance state. We define such a state as an eigenfunction of an approximate molecular Hamiltonian which includes all terms except those which couple the bound states to the translation continua. Thus intramolecular vibrational redistribution and nonradiative transitions other than fragmentation would be manifested only in the relative phases of the states included in the initial superposition created by the excitation. For the purposes of this discussion, we ignore the relative phase factors and consider only population loss from the bound states. Differences in the rate of appearance of fragments in different channels can be observed if the following two conditions are satisfied: (i) multiple resonances are excited simultaneously and (ii) relative coupling strengths of the resonance states to continua are different. It is easy to verify by a contrapositive argument that these are necessary conditions. The second criterion has to be quantified in order for the pair to be sufficient conditions as well.

The observed temporal evolution of population in each CN rotational state can be modeled as a single exponential buildup with the time constants for different N'' being equal within experimental error. At least one of the two conditions just stated is therefore not satisfied. Although our experiments cannot distinguish between the cases of one resonance state coupled to the continua and many such states equally coupled to the translational states, the former is an unlikely possibility because of energy redistribution (discussed in later sections), which leads to the excitation of multiple resonance states prior to reaction.

If we assume that many resonance states are populated by or following photoexcitation, the second condition insists that the coupling strengths are determined by the constants of motion—total energy and angular momentum. The possibility that only one state in the set of excited states dissociates can be ruled out on the basis of the single exponentials observed in transient absorption (see discussion below).

If the reaction were statistical in the reagent, rates of nonradiative decay and vibrational redistribution would be much faster than the rate of reaction. All quasidegenerate resonance states would be coupled to the optical state and to the dissociation continua. The discussion above makes no claim about the *extent* of redistribution, although experimental results suggest that all resonance states that are populated are equally coupled to products. Thus measurements of equal rates in different product channels indicate rapid redistribution among the set of resonance states which are coupled to the optical state. It is important to note this set does not necessarily include all accessible states.[35]

In our initial communication we reported rates changing as a function of CN(N''). At that time, we were unable to determine whether the observed dependence was a manifestation of nonstatistical effects or simply an ensemble effect. Our current results show unambiguously the latter is the correct interpretation of our previous study.

C. Initial angular momentum dependence

Figure 5 illustrates the effect of a finite spread in the distribution of initial energy and angular momentum. The photon energy promotes molecules in the vibrationally and rotationally cold ground state to states 25 cm^{-1} above the threshold for dissociation. If this were the maximum energy available for distribution among product degrees of freedom, the rotational quantum number of CN would be $N'' \leqslant 4$. Clearly, product channels with CN($N'' > 4$) must originate from internally excited NCNO. Since the distribution of vibrational states at low energies is sparse, we assume that most of the excitation is rotational.

These measurements dramatize the need for performing experiments in molecular beams where extensive cooling of

TABLE II. N'' dependent lifetimes of *warm* expansion (ps).

N''	Lifetime 1	Lifetime 2	Fraction
0	107	289	0.296
3	123	532	0.425
4	95	380	0.392
5	64	230	0.433
6	26	213	0.352
7	37	183	0.730

the internal degrees of freedom is achievable. They also support our claim above that the previously observed N'' dependence of the dissociation rates in a bulb was due to ensemble energy. In Table II we list the fitted rate constants for each transient with the fraction of the fast component to the total amplitude. It is not possible to accurately represent a distribution of rate constants with average values and this was reflected in the sensitivity of the fit to the initial guess. The values listed in the table are therefore the average of fitted values obtained with a range of initial guesses.

The observed quasibiexponential behavior in Fig. 5 reflects the dissociation of molecules from different J,K states. For molecules in high J, low K states, the centrifugal barrier is expected to be higher than for molecules in low J states. Accordingly, the dissociation rates from these states will be relatively slow. On the other hand, the dissociation rates for molecules in high $K(K \approx J)$ states should be faster. This is because the initial J (good quantum number) is converted to average l, especially if the rotational constants of the fragments are much larger than those of the reagent. States with high K are not as constrained with angular momentum conservation laws and behave more like vibrational states.

The results for the higher N'' channels corroborate the discussion above. The $N'' = 7$ channel is closed for energies less than 105 cm^{-1} so that only rotationally excited molecules ($J \geqslant 6$) can contribute. Table II shows that a significant fraction of molecules decay into this channel with rates $\sim 5 \times 10^9$ s^{-1} (slow component of the quasibiexponential), a value which is a factor of 2 smaller than the rate of dissociation of NCNO with ~ 100 cm^{-1} of excess vibrational energy and no rotational excitation. This slow component is derived from the high J, low K states. The fast component is faster than the rate measured in the cold expansion ($E_x = 105$ cm^{-1}), indicating the involvement of high $K(K \sim J)$ states. This ensemble effect was also observed in the lower N'' channels.

D. Energy redistribution and reaction mechanism

The model we adopt here is described in Fig. 12. The S_1 singlet level, which carries most of the oscillator strength, is quasidegenerate with many levels from S_0 and/or T states. Since the barrier to dissociation on S_1 is high (estimated to be more than 5000 cm^{-1} [6]), and the density of levels in $S_0^\dagger$ and $T^\dagger$ is appreciable, energy redistribution from the state of S_1 character to $S_0^\dagger$ (or $T^\dagger$) states is the primary step for dissociation. This intramolecular process requires electronic coupling between the initial and final states, which may involve promoting modes that mediate vibrational/rotational

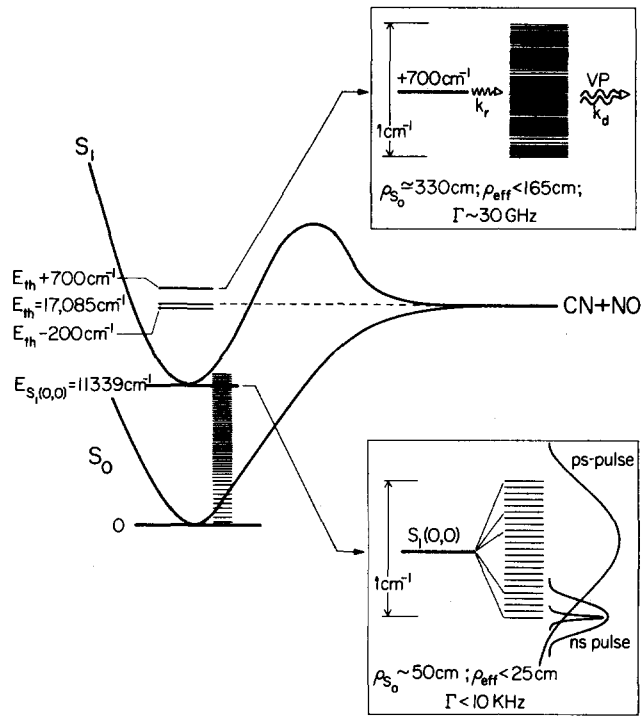

FIG. 12. A pictorial representation of energy redistribution, predissociation and the effect of coherent excitation. The lower right inset shows the detailed energy level structure near the S_1 origin. The "broad band" ps pulse can excite the state of S_1 character, whereas the ns ("narrow band") pulse cannot. The upper insert shows the structure above dissociation threshold. The greater density of states and lifetime broadening makes the spectrum of quasibound states appear continuous.

energy redistribution on the final state surface. The reaction proceeds from the final state surface. We therefore consider both processes (i.e., energy redistribution and dissociation) explicitly.

Below the dissociation threshold, the redistribution discussed here is quite similar to the case of intermediate sized molecules, such as pyrazine and isoquinoline.[37] As shown in the case of pyrazine, a picosecond pulse with a coherence width spanning the eigenstates of the system leads to the preparation of the zero-order state (or close to it), in this case the S_1 state. Intramolecular dephasing is the primary decay process (in pyrazine it was observed to be 100 ps[37]) which leads to the population of long-lived states, in this case the $S_0^\dagger$ (or $T^\dagger$) states. For NCNO near the S_1 origin, the vibrational density of states is $\rho_v \sim 50$ per cm^{-1}. The effective (including symmetry restrictions and limited couplings) density is less than 25 cm, ignoring rotations for the sake of simplicity. The linewidth of the states is < 10 kHz, indicating that below the dissociation limit, the spacing between levels is greater than the intrinsic width. The two-color picosecond transient absorption experiments reported here and the recent fluorescence lifetime measurements of Reisler *et al.*[38] support this view. Our transient absorption studies show (Fig. 7) a rise (< 8 ps) and no decay at longer times. The fluorescence experiment below threshold of Reisler *et al.*[36] determines the long decay component to be $> 100\,\mu$s. The laser coherence width in their case is probably less than 0.5 cm^{-1}, while in our picosecond experiments it is 3 cm^{-1}. Thus in the ns experiments one is measuring the

long-time ("dilution effect") decay of an eigenstate or a bunch of eigenstates (Fig. 12). The ps experiment coherently excites the distribution of eigenstates which following dephasing (ps's) produce the long-lived $S_0^\dagger$ (or $T^\dagger$) states that are subsequently probed in the transient absorption experiment. The early-time dephasing is also supported by the fact that below (or near) threshold the rotational structure of the absorption bands was not resolved using a 0.04 cm^{-1} bandwidth laser.[6] Finally, the difference (27 vs 3 cm^{-1}) in linewidths observed below threshold for different absorption bands could be due to the influence of the promoting mode(s) on electronic couplings of nearby states. This proximity effect is also found in isoquinoline S_1/S_2 coupling.[37]

Above the dissociation threshold the picture is somewhat different. For example at $E_{th} + 700$ cm^{-1}, $\rho_{eff} < 150$ per cm^{-1} and the linewidth (from our dissociation rate measurements) is ~30 GHz. Both the density and level width have increased considerably and the picture here is that of fast and reversible energy redistribution followed by predissociation (see Fig. 12). If we ignore coherence effects, then we can evaluate the relative importance of the redistribution vs predissociation rates. Simple kinetics indicate that the initial state S_1 decays by the redistribution rate constant (k_r):

$$S_1(t) = S_1(0)e^{-k_r t}$$

while $S_0(t)$ will build up and decay according to

$$S_0(t) = S_1(0)\frac{k_r}{k_r - k_d}(e^{-k_d t} - e^{-k_r t}) .$$

It is important to note that if $k_r - k_d$ is positive, the decay of $S_0(t)$ will be given by k_d. The product buildup in this limit ($k_r > k_d$) is simply given by

$$P(t) \approx S_1(0)(1 - e^{-k_d t})$$

and exhibits the same rate as $S_0(t)$, consistent with experimental observation. We have ignored reversible processes, since ρ is large and detailed balance implies very long recurrence times. The important point here is that the picosecond product appearance times, transient absorption decay rates and other spectroscopic data are all consistent with this model. This allows us to separate the redistribution from predissociation processes, within the context of the model, and to conclude that the measured rates are k_d. These k_d change by three orders of magnitude on going from near threshold to 700 cm^{-1} above threshold, yet the absorption spectrum still shows sharp features. The linewidth above dissociation threshold is given by the dephasing rate. An estimate of k_r is ~$(3\text{ ps})^{-1}$, which is still larger than the observed rates (ns^{-1} at threshold to 10 ps^{-1} at 700 cm^{-1} above threshold).

Finally, in the above discussion we tacitly ignored the contribution of the triplet state below S_1. This is not known for certain, although there are a number of points that may be presented in favor of the S_0 choice. First, if the triplet were involved in addition to S_0 then the product buildup should be a biexponential rise with the ratio of the two components of the rise determined by the relative redistribution rate constants to S_0 and T. This has not been observed in our experiments—all transient absorption decays and product buildup rates are matching single exponentials. Second, extensive perturbations of the levels of S_1 have been attributed to mixing with S_0.[6] ρ is ~280 cm in the ground state, compared to ~20 cm in T (assuming the same frequencies and that T is ~6000 cm^{-1} above S_0, which is not known for NCNO) at threshold. The choice of S_0 over T has been favored before for NCNO by Wittig's group. It is also interesting that in HNO, threshold dissociation proceeds via S_0.[30]

E. Reagent excess energy dependence

Figure 3 shows rate constants for the appearance of CN as a function of excess energy. A plot of the rates near threshold is presented in Fig. 13 with a smooth curve drawn through the data and extrapolated to lower energy to obtain the threshold energy for reaction. Scanning DL1 with DL2 tuned to probe CN($N'' = 0$), we were able to reproduce the results of Nadler *et al.* for excitation wavelengths shorter than 5853 Å. Relative positions of peaks and the absolute value of the threshold energy are in excellent agreement. The lifetimes vary smoothly from ⩾2 ns at 5853 Å to ~10 ps at 5630 Å. It is interesting to note that we do not observe the peak just at threshold. Previous experiments show evidence for very long appearance times (70–20 ns) corresponding to tunneling through a small rotational barrier.[6] Our experiments are not designed to measure the long rise times (~10 ns) close to threshold expected on the basis of previous work.

The rapid increase in the rates from threshold requires further consideration of the effect of finite spread in energy. Since the pump pulse has a finite spectral width (3 cm^{-1}), the initial ensemble is not strictly a microcanonical one, and the observed rates are larger than the rate at the mean energy. Molecules absorbing the redder photons have less total energy and therefore dissociate more slowly than the ones which absorb the bluer photons. There are two possible sources of bias in our measurements. At threshold, the reactive part of the ensemble has a skewed energy distribution and the average rate is faster than the rate of a true MC ensemble having the mean energy of the excitation pulse.

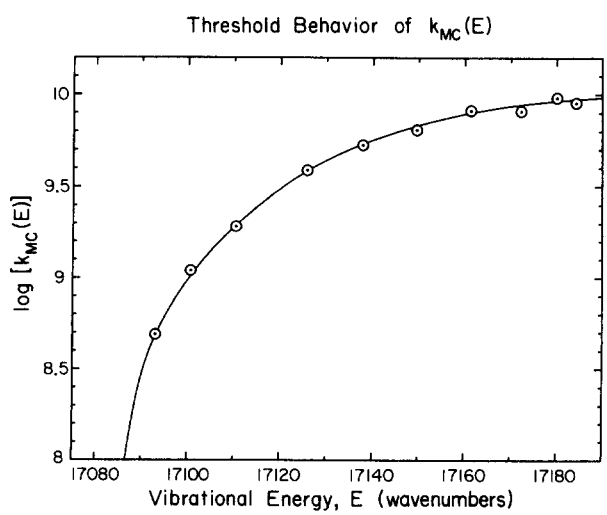

FIG. 13. Rates of dissociation measured near threshold showing the onset of reaction.

This effect becomes of lesser consequence if tunnelling effects are taken into account. The second point regarding threshold measurements is that the limited time range over which the appearance of products is measured constitutes a biased sampling of the ensemble (within 3 cm^{-1}). The severity of this unavoidable systematic error can be reduced simply by carrying out measurements to time delays of several τ. Since both of these effects are expected to be small in magnitude and nonnegligible only near threshold, we make no effort to adjust our results to correct for these errors.

Calculations of MC rates using PST and RRKM theory are compared with our rate measurements below, in an attempt at understanding their dependence on excess energy in the reagent.

1. Comparison with statistical theories: Phase space theory

Although it is well known that PST overestimates rates, we present results of these calculations as an upper bound for the observed rates at all energies. These rates should be a good approximation very close to threshold. The calculations were performed on a PDP 11/23 + computer using a Lennard-Jones attractive potential ($C_6 = 1.60\times10^5$ erg·Å^6). The molecular constants are collected in Table I.

It is crucial to assess all degeneracies for a correct absolute rate calculation. The total angular momentum is the sum of electron spin and orbital angular momentum, rotational angular momentum and nuclear spin. We assume that the nuclear spin coordinates are separable and the total nuclear spin is conserved independently. As the dissociated fragments are distinguishable, the Pauli principle imposes no restrictions on possible combinations of angular momentum quantum numbers in the products. The total angular momenta of the fragments are good quantum numbers and are easily computed. In a singlet state electron spin is zero and the total angular momentum of NCNO is the spectroscopically assigned quantum number J. The phase space volume for the transition state is estimated using Eq. (8). The two spin–orbit states of NO are treated as independent channels with equal weighting.

We have performed a full PST calculation ($\kappa = 1$) and the results are shown in Fig. 14 (curve C). We also make an attempt at conserving electronic quantum numbers by proposing a value less than unity for κ, the transmission coefficient. Ignoring differences in electronic energy in the products, we notice an eightfold degeneracy for a given combination of CN and NO rotational states. This arises from a twofold degeneracy of the electron spin in each of the two fragments and an additional twofold degeneracy (λ-doubling) of the electron orbital motion in NO. Each combination of electronic quantum numbers should correlate with a different electronic state of NCNO. As discussed in Sec. V A 3, some combinations correlate with the triplet and excited singlet states and therefore represent closed channels. Correlation between the states of the two radicals and a linear NCNO can be made, but enough information for detailed correlations to the bent NCNO is not available. If we take recourse in statistical adiabaticity, i.e., on the average these quantum numbers are preserved, only one-eighth of all

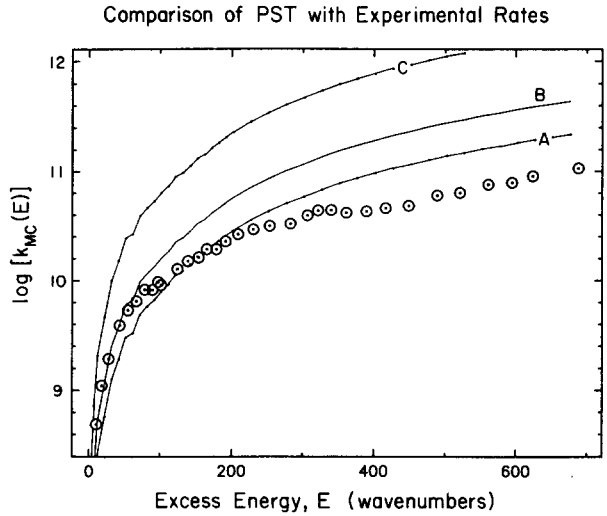

FIG. 14. Comparison of PST theory with experiment. Calculated rates ($J = 3$) are shown as connected lines. Curves A, B, and C correspond to $\kappa = \frac{1}{8}$, $\frac{1}{4}$, and 1, respectively. The density of states was approximated by the Whitten–Rabinovitch method for harmonic vibrations and summed over allowed K. The circles are the experimentally measured values. Note that the structure is somewhat deemphasized because the rates are plotted on a logarithmic scale.

final states correlate with the ground singlet state. This is implemented in our calculations by setting $\kappa = \frac{1}{8}$. It must be emphasized that the full count ($\kappa = 1$) includes all electronic degeneracies in the products, in particular the spin states of CN and the orbital degeneracy of NO(Π). These states have to be considered explicitly because the total angular momentum of each product is important for momentum conservation, while the energy can be approximately represented by the spectroscopic "good" quantum numbers.

The domain of applicability of this choice needs some consideration. The value $\frac{1}{8}$ was chosen assuming the electronic quantum numbers do not appear in the energy expression except as small corrections that may be neglected to a good approximation. In reality, spin–orbit interaction in NO is nonzero (~ 120 cm^{-1}). In the energy range 0–120 cm^{-1} above threshold, the electronic degeneracy is effectively 4, rather than 8. Therefore $\kappa = \frac{1}{4}$ should be used in this range, while at higher energies $\kappa = \frac{1}{8}$ is more appropriate. It should be noted that the transmission coefficient is expected to be a continuous function of energy and the change from 0.25 to 0.125 is likely to occur over a range of energies. Curves A and B in Fig. 14 were calculated with $\kappa = \frac{1}{8}$ and $\frac{1}{4}$ respectively, but it should be emphasized that this is done simply to illustrate the effect of $\kappa < 1$ on the PST calculation of rates.

The density of states was calculated using the Whitten–Rabinovitch approximation for harmonic vibrations.[16] For $J = 0$, the vibrational state density in S_0 at threshold was ~ 280 per cm^{-1}, which is large enough for the approximation to be valid. The density was corrected for contributions from states with different values of K with the formula

$$\rho(E,J) = (2J+1)\sum_{K=0,J}\sigma\rho_v[E - B''J(J+1) - (A''-B'')K^2], \quad (14)$$

where $\sigma = 1$ for $K = 0$, and $\sigma = 2$ otherwise. $\rho(E,J)$ is the total density of rovibrational states at energy E that have angular momentum J. In contrast to Eq. (8), this expression displays all degeneracies $(2J + 1)$. $\rho_v(E,J,K)$ is the subset of ρ containing only states having K as the projection of J along the figure axis. Thus ρ is simply the sum over all allowed K of ρ_v.

In Fig. 14, calculated rates using different values of κ are superimposed on a plot of $\log k_{MC}(E)$ vs E. The agreement between theory and experiment is reasonable at low energies. Clearly the range of energy over which κ changes its value is small and occurs where $E \approx \Delta E_{so}$. At the high end of the energy range studied, PST rates are indeed higher than the measured rates. It should be emphasized that ρ was calculated using the harmonic approximation. Spectroscopic studies demonstrate that the bending potentials are quite harmonic.[28] The value of C_6 was chosen for consistency with the calculations which reproduced the measured PSDs.[6] Sample calculations show that decreasing or increasing its value by an order of magnitude does not affect the rates significantly. Finally, the same algorithm used for calculating rates was used to produce the PSD obtained in Ref. 6, and good agreement was found.

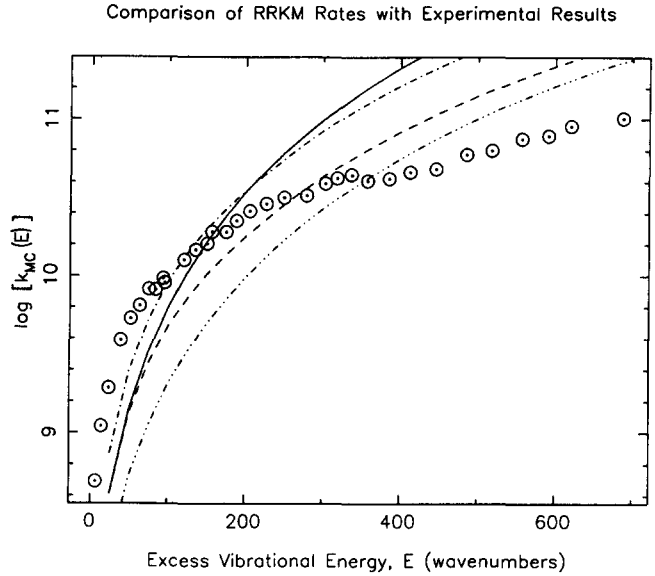

FIG. 15. Comparison of RRKM theory with experimental results. The densities were obtained as for the PST calculations. $N^\dagger$ was obtained from a direct quantum count of harmonic vibrations. The different connected lines correspond to different combinations of frequencies (see Table III). The following representation is used: model A (—), model B (- - -), model C (– · –), and model D (– · · · –).

2. RRKM rates

A standard RRKM calculation using only vibrational frequencies of the reactant yields a discontinuous distribution of rates as a function of energy and is obviously incorrect. We attempt to model the transition state in the following way. We choose the frequencies for the CN and NO stretch modes to be equal to their free radical values. The three bending motions are represented by three harmonic oscillators of very low frequency (see Table III). The reaction coordinate is the central bond stretch mode. The vibrational zero-point energies are assumed to have been included in the threshold energy. The rotational constants are estimated for the equilibrium geometry with an extended central bond. $N^\dagger(E)$ was calculated using a direct count algorithm[39] with no symmetry restrictions and the densities were obtained using the semiclassical approximation as in the previous section. Angular momentum was conserved by holding J constant. For a given energy, a sum over K analogous to Eq. (14) was used:

$$N^\dagger(E^\dagger,J) = (2J+1) \sum_{K=0,J} \sigma N_v^\dagger(E^\dagger - B^\dagger J(J+1) - (A^\dagger - B^\dagger)K^2),$$

where $E^\dagger$ is the difference of the total energy (E) and the dissociation energy (including zero point energies). σ is as in Eq. (14) and $N^\dagger$ is the total number of rovibrational states with energy less than or equal to the total energy and having angular momentum J. $N_v^\dagger$ is a subset of these states whose angular momentum has a projection K along the figure axis. Note that we have implicitly assumed the TS is a symmetric top. Varying $A^\dagger$ and $B^\dagger$ changes the results by a small amount.

TABLE III. Frequencies in model TS for RRKM calculations.

TS rotational constants (cm^{-1}): A = 2.0, B = 0.015, C = 0.015			
TS Vibrational frequencies (cm^{-1}):			
Model A	Model B	Model C	Model D
1904	1904	1904	1904
2068	2068	2068	2068
10	10	5	20
12	12	12	25
50	200	200	50

Some representative cases are shown in Fig. 15. The frequencies used in these calculations are listed in Table III. It is apparent that a TS with harmonic frequencies is unable to reproduce experimental results. With very low frequencies, the low energy behavior can be approximated at the cost of reasonable agreement at higher energies and vice versa. This is not too surprising since a loose transition state, as proposed on the basis of PSDs and supported by our PST calculations, will imply larger separation between energy levels at higher quantum numbers. This is a crude method for modeling a loose transition state and should be considered in that spirit only since the number of possible choices is quite large. A proper treatment using a recent modification of the theory developed for flexible transition states of arbitrary looseness is currently in progress.

Although neither PST nor RRKM models can quantitatively account for the observed results, the general trend shows that the TS is indeed fairly loose. This is clearly borne out by the small harmonic frequencies we have to assume in the RRKM model to obtain rates having the correct order of magnitude.

It has been conjectured that PST predictions of the rate will be accurate at energies close to threshold but that the infinitely loose TS is not a good approximation at higher energies. This statement borrows from concepts of the vari-

ational theories—the exact location of the TS changes with the energy available for reaction. If the dissociation of NCNO were a simple process that could be described as a fast redistribution of vibrational energy and slow (adiabatic) passage through a single dividing surface, PST should reproduce the experimental results. We showed that the effects of electronic correlation could be accounted for by simple heuristic arguments very close to threshold. The position of the dividing surface changes slowly and continuously with increasing energy, provided the reaction remains direct, i.e., a single dividing surface exists such that any trajectory intersects it at most once. The ratio of the observed rates and PST rates may be interpreted as an energy dependent transmission coefficient $\kappa(E)$, and is plotted in Fig. 16 for this purpose. The first few points have been corrected for tunneling ($10^8\ s^{-1}$) and the corresponding PST rates averaged over a Boltzmann distribution of rotational states at 2 K. The gradual change in $\kappa(E)$ with increasing energy can be interpreted as reflection of a smooth transition from a completely loose to a tighter TS.

3. Structure in the excess energy dependence

The plot of the rates vs excess energy (Fig. 3; see also Fig. 15) shows an inflexion and a weak maximum around $320\ cm^{-1}$. Although no conclusive interpretation of this unusual behavior can be made at this time, we discuss several plausible explanations. Detailed knowledge of the PES(s) is required to identify which of these possibilities most closely resembles nature.

PST and RRKM theory assume a radially isotropic potential. In reality, NO and CN have permanent dipole moments and the long range potential is determined by dipole–dipole interaction which is dependent on their relative orientation. In the limiting cases of linear approach, head-to-head or head-to-tail, the electrostatic potential is repulsive in one case and attractive in the other. The central bond stretching motion would not be separable and the proper reaction coordinate would be some complicated motion with projection along multiple normal modes. Estimating proper statistical rates for such a system is not a tractable problem as yet.

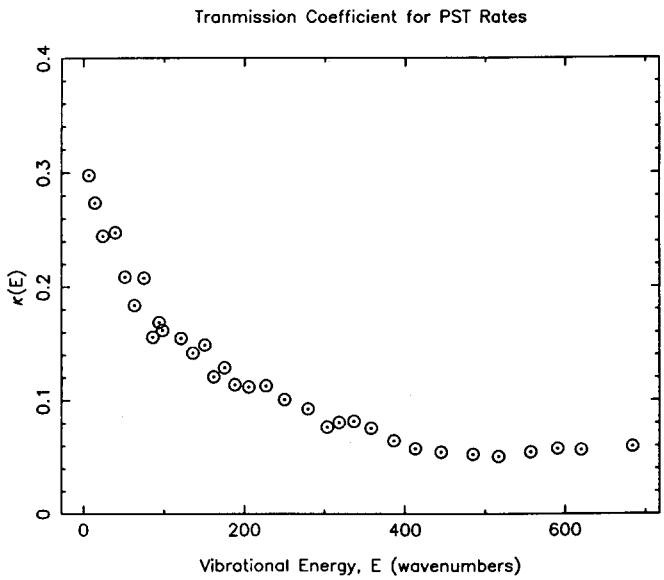

FIG. 16. The energy dependent transmission coefficient of PST rates. The first two data points near threshold are corrected for the distribution in internal energies at 2 K.

Related to the radial anisotropy of the PES is the possibility of complex formation and reactions leading to other products. One postulated reaction[40] is

$$NCNO \rightarrow [NC{\cdot}ON] \rightarrow N_2 + CO\,.$$

Loss of NCNO into this channel would be manifested in the rate of CN production, but not necessarily in the relative distributions of $CN(N'')$. A cyclic intermediate has been proposed as a transient species along the exoergic path for CO production. The distribution of energy in the internal and translational degrees of freedom in a particular channel will reflect the existence of other product channels as will the absolute rates. PSDs in a given channel will be affected by the global shape of the PES only if trajectories entering the channel may return to the reactant region of phase space.

The experimental results could be presented from an operational perspective. All simple theories predict a smooth monotonic dependence of the rates on energy. Such an empirical curve drawn to approximate the data at the high energy end of the range studied underestimates the rates in the range 200 to $400\ cm^{-1}$. A simple interpretation of the enhanced rates is that the vibrational phase space is restricted. The maximum at $\sim 320\ cm^{-1}$ would then correspond to the energy regime for transition from restricted to complete redistribution in the reactant and the close agreement between PST and the data at low energies is fortuitous. The statistical adiabatic channel model considers strict conservation of vibrational quantum numbers of those motions which can be clearly identified in reactants and products. In this reaction, they are the terminal CN and NO stretches. From an extension of this idea, one could conceive of the restrictions in reactant phase space being due to weak coupling between these modes and the others. This picture does not contradict the observation of equal appearance times in all product channels and the transient absorption measurements if we assume that redistribution cannot populate these modes directly. Some fluctuations in the rate is expected as the nature of the optical state changes with the photon energy in the transition regime, which may explain the observed structure in $k_{MC}(E)$.

Although the involvement of other electronic states as direct channels of reaction have been argued against, they may be important in determining the shape of the S_0 PES in the reaction channel. It is believed that S_1 and T_1 correlate with ground state CN and NO. Spin–orbit coupling may induce mixing between the vibronic manifolds of S_0 and T_1, leading to avoided crossings and multiple minima (Demkov resonances) along the reaction coordinate.[41] Similar effects would also arise from interactions between the manifolds of the two singlet surfaces. It must be noted that such minima can occur only if some vibrations are adiabatic, i.e., redistribution is not complete among all vibrational modes. This may be visualized as dynamical trapping, molecules vibrating in a particular mode see potential minima greater in number and different in position than molecules executing a

different form of vibrational motion. The purely electronic S_0 PES cannot have a minimum along the reaction path (except at the equilibrium geometry of the reactants) and the rates can be compared to PST or RRKM for energies such that only this surface is important. At energies greater than 200 cm^{-1}, the reaction must then proceed through multiple transition states. The complex mode of the reaction should manifest itself in the absolute rate, but not necessarily in PSDs. The rates may be estimated only if the contribution from each adiabatic PES (electronic and vibrational) can be estimated.

It is interesting to note that there is no obvious correlation between the sharp features in the absorption (photodissociation yield) spectrum and the structure in $k_{MC}(E)$. In the bimolecular scattering of ground-state CN and NO radicals, fluctuations in the scattering cross section corresponding to orbiting or compound (Feshbach) resonances may be present.[42] In this example of predissociation, the reaction is initiated in such compound states at all energies. Structure in the unimolecular rate as a function of energy is therefore a manifestation of restrictions to the redistribution of energy.

4. Rates vs product state distributions

Although a complete interpretation of the energy dependence of the rates is not possible without a proper description of the PES in full detail, we can assert that the dissociation rates are sensitive to different aspects of the potential than PSDs. Nascent distributions obtained under similar experimental conditions for CN and both spin–orbit states of NO are in good agreement with PST, with no evidence of restricted IVR or nonadiabatic effects. Comments on the intrinsic differences between measurements of rates and PSDs are clearly appropriate.

Absolute reaction rates are affected by the global features of the PES, in contrast to PSDs. Reactive channels which do not yield CN and NO as products are not presented in the PSDs of CN (or NO) but will be manifested in the absolute rate. In other words, the total yield in the CN + NO channel will be affected by the presence of other, chemically distinct, open channels, even though the relative population of product quantum numbers within a single rearrangement channel might not be influenced.

There are also subtle considerations in a single channel which influence rates and PSDs differently. Rates are thought to be determined by a hypothetical surface in phase space that minimizes the flux of trajectories through it. This dynamic bottleneck to reaction may be located somewhere other than at the maximum (saddle point of PES) of V_{eff} [Eq. (7)]. PSDs are determined at this critical point which is generally further toward products than S_m. An equivalent statement is that exit channel effects (long range collisions) are important for this reaction, even near threshold. As the energy available for reaction increases, the position of the TS (S_m) migrates slowly towards the reagent, thus accentuating the differences between PSDs and rates. The rates are sensitive to IVR and the short-range interactions on the PES, while product state distributions are mapping long-range influences and impact parameter distributions. This is strong motivation for examining photofragmentation on ultrashort timescales.

VI. CONCLUSIONS

This paper, the first in the series, presents direct measurements of state-to-state rates (and product state distributions) of the dissociation of beam-cooled NCNO as a function of reagent and product energy. The studies provide an opportunity for examining the picosecond time-resolved dynamics of this reaction. The primary experimental findings reported here are:

(a) State-to-state rate constants are found to be independent of the character of the final product rotational state. A simple model is used to argue that energy randomization is fast in the accessible (subject to energy and possibly dynamical constraints) region of phase space.

(b) Rates as a function of energy exhibit a threshold (17 083 cm^{-1}, the bond energy, 48.8 kcal/mol) and increase with total energy in the reagent. The functional dependence of the rates on energy is not strictly monotonic but shows some structure, which cannot be explained using simple statistical theories. Comparison with RRKM and PST provides insight into the nature of the transition state and the effects of recoil during fragmentation.

(c) Transient absorption measurements show a population decay at a rate equal to the buildup of products. In the light of these experiments, we consider energy redistribution and predissociation explicitly. It is reasoned that only one potential energy surface is important at the energies considered.

(d) Differences between product state distributions (statistical – PST) and absolute rates (nonstatistical) are rationalized as manifestations of the global vs local features of the PES, or early-time vs long-time dynamics of the reaction process. *Ab initio* or semiempirical calculations of the full S_0 PES would be of great use in gaining further insight into this prototype and elementary reaction.

ACKNOWLEDGMENTS

This research was supported by a grant from the National Science Foundation (CHE-8512887). Some initial support was provided by the President's Fund and the Keck Foundation. We thank Professor R. B. Bernstein and Professor R. A. Marcus for many illuminating discussions. We also wish to thank Professor C. Wittig and Professor H. Reisler, and Dr. M. Noble for many helpful discussions throughout this work and assistance in the safe and successful synthesis of NCNO. We are particularly grateful to Dr. Hanna Reisler for communicating her results on the fluorescence lifetime and for an indepth discussion of NCNO dissociation.

APPENDIX: CHARACTERISTIC CONSTANTS FROM PUMP–PROBE TRANSIENTS

In cases where the dynamics occur on a time-scale much longer than the duration of the excitation or probe pulses,

the experimental response can be analyzed without explicitly accounting for their finite temporal widths. More accurate estimates of the constants of the molecular response are obtained if the instrumental response function is included in the analysis. The problem has been solved in the context of fluorescence lifetime measurements by photon-counting techniques[43] and is given by a convolution integral, and in transient absorption experiments.[44] Here, we show explicitly that a pump–probe transient may also be analyzed by a mathematically similar form, which we utilize in the analysis of our data.

First, we consider the effect of the excitation pulse which has a temporal profile, $f(t)$. If the molecular response has a functional form $M(t-t_0)$, the measured response, $S(t)$, is represented by the Riemann sum over the range with $f(t)$ nonzero:

$$S(t) = \sum_n f(n\delta\tau)\cdot M(t-n\delta\tau)\,. \tag{A1}$$

In the limit of infinitesimal $\delta\tau$ the sum is the definite integral in Eq. (A2), which can be recognized as a convolution integral of f with M:

$$S(t) = \int_{-\infty}^{t} f(\tau)M(t-\tau)d\tau\,. \tag{A2}$$

In a pump–probe scheme where both pulses have finite temporal spread, the time parameter is generally chosen to be the peak-to-peak delay, T. Including the probe pulse in Eq. (A2) results in

$$S(T) = \int_{-\infty}^{+\infty}\int_{\tau_1}^{+\infty} f_1(\tau_1)M(\tau_2-\tau_1)\,f_2(\tau_2-T)d\tau_2\,d\tau_1\,.$$

Defining a new variable $\tau' = \tau_2 - T$,

$$S(T) = \int_{-\infty}^{+\infty}\int_{\tau_1-T}^{+\infty} f_1(\tau_1)M(\tau'-\tau_1+T) \times f_2(\tau')d\tau'\,d\tau_1\,.$$

Another substitution $s = \tau_1 - \tau'$ and a change in the order of integration results in

$$S(T) = \int_{-\infty}^{T}\int_{-\infty}^{+\infty} f_1(\tau_1)\,f_2(\tau_1-s)M(T-s)d\tau_1\,ds\,.$$

The system response function, $R(t)$, obtained by setting $M(t)$ equal to the Dirac delta-function is seen to be the cross correlation of the two pulses. This shows that the cross-correlation function is indeed the true system response function

$$R(T) = \int_{-\infty}^{+\infty} f_1(\tau_1)\,f_2(\tau_1-T)d\tau_1\,.$$

The measured molecular transient can then be written as in Eq. (A3):

$$S(T) = \int_{-\infty}^{T} R(s)M(T-s)ds. \tag{A3}$$

In our experiments, $M(x)$ has the form of an exponential buildup. Next, we show that the convolution of a pulse with zero amplitude at long positive and negative times with an exponential rise is identical to the convolution of the integral of that response with an exponential decay. In other words, we want to show that the following equality holds:

$$\int_{-\infty}^{t} f(\tau)A\,[1-e^{-k(t-\tau)}]d\tau = \int_{-\infty}^{t}\left(\int_{-\infty}^{\tau} f(s)ds\right)A'e^{-k(t-\tau)}d\tau\,.$$

The right-hand side can be integrated by parts:

$$\begin{aligned}\int_{-\infty}^{t}\left(\int_{-\infty}^{\tau} f(s)ds\right)A'e^{-k(t-\tau)}d\tau &= A'e^{-kt}\left[\int_{-\infty}^{\tau} f(s)ds\cdot\frac{e^{k\tau}}{k}\Big|_{-\infty}^{t}\right.\\ &\quad\left.-\int_{-\infty}^{t}\frac{e^{k\tau}}{k}\cdot\frac{d}{d\tau}\left(\int_{-\infty}^{\tau} f(s)ds\right)d\tau\right]\\ &= A'e^{-kt}\left[\int_{-\infty}^{t} f(s)ds\cdot\frac{e^{kt}}{k}-\int_{-\infty}^{t}\frac{e^{k\tau}}{k}f(\tau)d\tau\right]\\ &= \frac{A'}{k}\int_{-\infty}^{t} f(\tau)[1-e^{-k(t-\tau)}]d\tau\,.\end{aligned}$$

This shows that the deconvoluted lifetimes are the same, but the amplitude is changed by a multiplicative factor. This has to be accounted for in deriving the correct fraction for a multicomponent rise. For a biexponential rise deconvoluted using the integrated pulse method, the correct ratio F of the amplitude of the fast component to the total amplitude is related to the fraction obtained in the fit F' by

$$F = \frac{k_2F'}{k_1(1-F')+k_2F'}\,,$$

where the exponential constants satisfy $k_1 > k_2$.

[1](a) J. L. Knee, L. R. Khundkar, and A. H. Zewail, J. Chem. Phys. **82**, 4715 (1985); (b) **83**, 1996 (1985); (c) J. Phys. Chem. **89**, 4659 (1985); (d) N. F. Scherer, F. E. Doany, A. H. Zewail, and J. W. Perry, J. Chem. Phys. **84**, 1932 (1986).

[2]N. F. Scherer, J. L. Knee, D. D. Smith, and A. H. Zewail, J. Phys. Chem. **89**, 5141 (1985).

[3]N. F. Scherer and A. H. Zewail, J. Chem. Phys. **87**, 97 (1987).

[4]J. L. Knee, L. R. Khundkar, and A. H. Zewail, J. Chem. Phys. **87**, 115 (1987).

[5]See, e.g., R. B. Bernstein, *Chemical Dynamics via Molecular Beams and Laser Techniques* (Clarendon, Oxford, 1982).

[6]I. Nadler, M. Noble, H. Reisler, and C. Wittig, J. Chem. Phys. **82**, 2608 (1985); I. Nadler, J. Pfab, H. Reisler, and C. Wittig, *ibid.* **81**, 653 (1984); I. Nadler, J. Pfab, G. Radhakrishnan, H. Reisler, and C. Wittig, *ibid.* **79**, 2088 (1983); C. Wittig, I. Nadler, H. Reisler, M. Noble, J. Catanzarite, and G. Radhakrishnan, *ibid.* **83**, 5581 (1985); C. X. W. Qian, M. Noble, I. Nadler, H. Reisler, and C. Wittig, *ibid.* **83**, 5573 (1985).

[7]E. P. Ippen and C. V. Shank, *Topics in Applied Physics* (Springer, New York, 1984), Vol. 18.

[8]P. Horsewood and G. W. Kirby, Chem. Comm. **1971**, 1139.

[9]J. R. Morton and H. W. Wilcox, Inorg. Synth. **IV**, 48 (1953).

[10]*Spectroscopic Data*, edited by S. N. Suchard (Plenum, New York, 1975), Vol. 1.

[11]I. Nadler, H. Reisler, M. Noble, and C. Wittig, Chem. Phys. Lett. **108**, 115 (1984).

[12]D. W. Marquardt, SIAM **11**, 431 (1964); David P. Millar, Ph.D. dissertation, California Institute of Technology, 1982.

[13]P. R. Bevington, *Data Reduction and Error Analysis for Physical Sciences* (Academic, New York, 1981).

[14]See, e.g., P. Brumer and M. Shapiro, Adv. Chem. Phys. **60**, 371 (1985); F. H. Mies and M. Krauss, J. Chem. Phys. **43**, 4455 (1966); S. A. Rice, in *Excited States*, edited by E. C. Lim (Academic, New York, 1975), Vol. 2, p. 111.

[15]L. D. Landau and E. M. Lifschitz, *Nonrelativistic Quantum Mechanics* (Pergamon, New York, 1982).
[16]W. Forst, *Theory of Unimolecular Reactions* (Academic, New York, 1973); P. J. Robinson and K. A. Holbrook, *Unimolecular Reactions* (Wiley–Interscience, London, 1974).
[17]See, for example, W. H. Miller, J. Chem. Phys. **65**, 4343 (1976).
[18]W. A. Wong and R. A. Marcus, J. Chem. Phys. **55**, 5625 (1971); D. L. Bunker and M. Pattengil, *ibid.* **48**, 772 (1968).
[19]P. Pechukas and J. C. Light, J. Chem. Phys. **42**, 3281 (1965); P. Pechukas, R. Rankin, and J. C. Light, *ibid.* **44**, 794 (1966); C. Klotz, J. Phys. Chem. **75**, 1526 (1971); C. Klotz, Z. Naturforsch, Teil A **27**, 553 (1972); W. Chesnavich and M. Bowers, J. Chem. Phys. **66**, 2306 (1977).
[20]The expression for $N^{\dagger}$ or ρ is for a specific value of J_z. The degeneracy associated with this quantum number appears in both numerator and denominator in Eq. (4) and therefore cancels out. For details, see Refs. 6 (Wittig *et al.*) and 19.
[21]S. W. Benson and D. M. O'Neil, *Kinetic Data for Gas Phase Unimolecular Reactions*, Natl. Bur. Stand. (U.S.) 21 (1970).
[22]M. Quack and J. Tröe, Ber. Bunsenges. Phys. Chem. **78**, 240 (1974); **79**, 170 (1975); M. Quack, J. Phys. Chem. **83**, 150 (1979).
[23]See, e.g., E. Pollak, in *Theory of Chemical Reaction Dynamics*, edited by M. Baer (Chemical Rubber, Boca Raton, FL, 1985); D. L. Bunker, J. Chem. Phys. **40**, 1946 (1964); W. L. Hase, J. Phys. Chem. **90**, 365 (1986).
[24]See, e.g., D. G. Truhlar and B. C. Garrett, Ann. Rev. Phys. Chem. **35**, 159 (1984).
[25]D. M. Wardlaw and R. A. Marcus, J. Chem. Phys. **83**, 3462 (1985); D. M. Wardlaw and R. A. Marcus, Chem. Phys. Lett. **110**, 230 (1984).
[26]R. Dickinson, G. W. Kirby, J. G. Sweeny, and J. K. Tyler, J. Chem. Soc. Faraday Trans. 2 **74**, 1393 (1978).
[27]B. Bak, F. M. Nicolaisen and O. J. Nielsen, J. Mol. Struct. **51**, 17 (1979); J. Pfab, Chem. Phys. Lett. **99**, 465 (1983).
[28]M. Noble, I. Nadler, H. Reisler, and C. Wittig, J. Chem. Phys. **81**, 4333 (1984).
[29]G. Herzberg, in *Molecular Spectra and Molecular Structure* (Van Nostrand, New York, 1965).
[30]R. N. Dixon, K. B. Jones, M. Noble, and S. Carter, Mol. Phys. **42**, 455 (1981); R. N. Dixon, M. Noble, C. Taylor, and M. Delhoume, Faraday Discuss. Chem. Soc. **71**, 125 (1981).
[31]H. W. Kroto, *Molecular Rotational Spectroscopy* (Wiley–Interscience, London, 1975).
[32]*Landolt–Börnstein, Physical Constants for Atoms and Molecules* (Springer, Berlin, 1983), Part II (Sup.).
[33]See, e.g., G. M. McClelland, K. L. Saenger, J. J. Valentini, and D. Herschbach, J. Phys. Chem. **83**, 947 (1975).
[34](a) M. Dupuis and W. A. Lester Jr., J. Chem. Phys. **83**, 3990 (1985); (b) M. Marudarajan and G. Segal, Chem. Phys. Lett. **128**, 1 (1986).
[35]In the language of classical mechanics, trajectories with initial conditions specified by the excitation do not fill the entire phase-space.
[36]H. Reisler, private communication [see Ref. 34(b)].
[37]See, e.g., P. M. Felker and A. H. Zewail, Chem. Phys. Lett. **128**, 221 (1986), and references therein; J. L. Knee, L. R. Khundkar, and A. H. Zewail, J. Phys. Chem. **89**, 3201 (1985).
[38]C. X. Qian, A. Ogai, H. Reisler, and C. Wittig (private communication).
[39]L. R. Khundkar, R. A. Marcus, and A. H. Zewail, J. Phys. Chem. **87**, 2473 (1983).
[40]B. G. Gowenlock and L. Radom, Aust. J. Chem. **31**, 2349 (1978).
[41]M. S. Child, in *Atom–Molecule Collision Theory*, edited by R. B. Bernstein (Plenum, New York, 1979).
[42]R. B. Bernstein, Phys. Rev. Lett. **16**, 385 (1966); R. J. LeRoy and R. B. Bernstein, J. Chem. Phys. **54**, 5114 (1971).
[43]See, e.g., D. V. O'Connor and D. Phillips, in *Time-Correlated Single Photon Counting* (Academic, London, 1984).
[44]See, e.g., B. I. Greene, R. M. Hochstrasser, and R. B. Weisman, J. Chem. Phys. **70**, 1247 (1979).